A P2rx7 Passenger Mutation Affects the Vitality and Function of T cells in Congenic Mice

Marco Er-Lukowiak, Yinghui Duan, François Rassendren, Lauriane Ulmann, Annette Nicke, Friederike Ufer, Manuel A Friese, Friedrich Koch-Nolte, Tim Magnus, Björn Rissiek

iScience

CellPress
OPEN ACCESS

Article

A *P2rx7* Passenger Mutation Affects the Vitality and Function of T cells in Congenic Mice

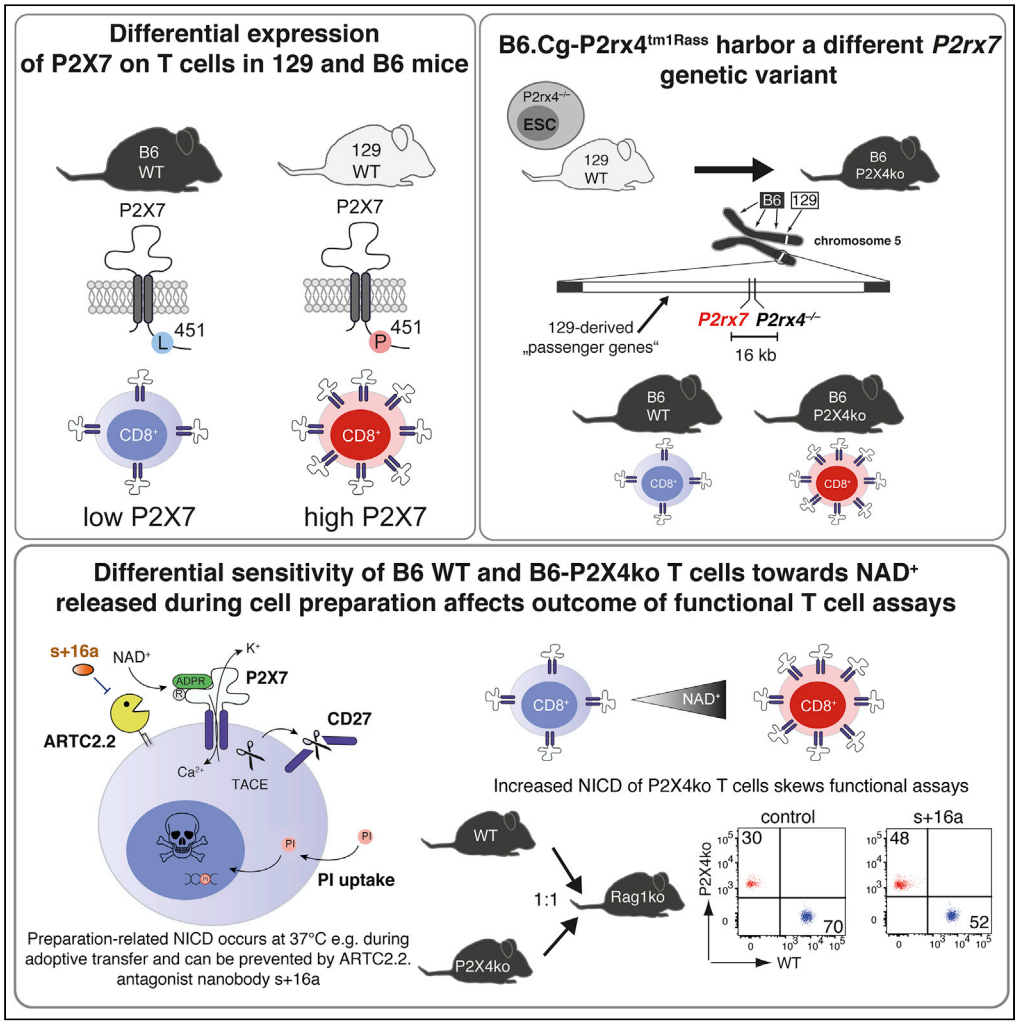

Marco Er-Lukowiak, Yinghui Duan, Francois Rassendren, ..., Friedrich Koch-Nolte, Tim Magnus, Björn Rissiek

b.rissiek@uke.de

HIGHLIGHTS

T cells from 129 mice express higher level of P2X7 compared with T cells from B6 mice

P2rx4^{tm1Rass} T cells express high level of P2X7 due to a *P2rx7* passenger mutation

P2rx4^{tm1Rass} T cells are highly susceptible to NAD-induced cell death (NICD)

NICD susceptibility of P2rx4^{tm1Rass} T cells confounds the outcome of functional assays

Er-Lukowiak et al., iScience *23*, 101870
December 18, 2020 © 2020 The Author(s).
https://doi.org/10.1016/j.isci.2020.101870

iScience

CellPress
OPEN ACCESS

Article

A *P2rx7* Passenger Mutation Affects the Vitality and Function of T cells in Congenic Mice

Marco Er-Lukowiak,[1] Yinghui Duan,[1] Francois Rassendren,[2,3] Lauriane Ulmann,[2,3] Annette Nicke,[4] Friederike Ufer,[5] Manuel A. Friese,[5] Friedrich Koch-Nolte,[6,7,8] Tim Magnus,[1,7,8] and Björn Rissiek[1,7,8,9,*]

SUMMARY

Among laboratory mouse strains many genes are differentially expressed in the same cell population. As consequence, gene targeting in 129-derived embryonic stem cells (ESCs) and backcrossing the modified mice onto the C57BL/6 background can introduce passenger mutations in the close proximity of the targeted gene. Here, we demonstrate that several transgenic mice carry a *P2rx7* passenger mutation that affects the function of T cells. By the example of P2rx4^{tm1Rass} we demonstrate that P2X4ko T cells express higher levels of P2X7 and are more sensitive toward the P2X7 activators ATP and NAD$^+$, rendering these cells more vulnerable toward NAD-induced cell death (NICD) compared with wild type (WT). The enhanced NICD sensitivity confounded functional assays e.g. cytokine production and cell migration. Our results need to be considered when working with P2rx4^{tm1Rass} mice or other 129-based transgenic strains that target *P2rx7* neighboring genes.

INTRODUCTION

In the pre-CRISPR-Cas9 era, gene targeting, in order to generate "knockout" or "knockin" mice, was often conducted in embryonic stem cells (ESCs) derived from 129-originating mouse strains. The obtained transgenic mice were then backcrossed on C57BL/6, the most widely used strain in immunological research. Because of genetic linkage, however, flanking regions of the targeted gene are unlikely to be exchanged by backcrossing, and the likelihood of exchange decreases the closer these regions are located to the targeted gene (Lusis et al., 2007). Genetic distances are often given in centimorgans (cM), with 1 cM distance representing the equivalent to 1% probability of two loci being separated during homologous recombination in the context of meiosis. In the mouse, 1 cM is, on average, equivalent to 2,000 kilobases; however, the rate of equivalence can vary greatly due to numerous factors (Silver, 1995). This implicates a probability of about 90% that upon backcrossing for 10 generations; a flanking region with a distance of 1 cM to the targeted gene is still of donor origin (Berghe et al., 2015; Lusis et al., 2007). Gene expression can vary in cells from different laboratory mouse strains and some mouse strains even constitute "natural knockouts" for certain genes e.g. if mutations or SNPs introduce premature STOP codons (Mostafavi et al., 2014). If such a differentially expressed or inactive gene is in close proximity of a targeted gene in 129 ESCs, backcrossing to C57BL/6 will introduce an experimental bias, because the differentially expressed/inactive gene most likely will be retained. A prominent example is the 129-derived Casp1 knockout mouse (e.g. Casp1^{tm1Flvw}). The 129 mouse strains carry a defective *Casp11* gene in the close proximity of *Casp1*, and the strong resistance to lethal lipopolysaccharide (LPS) injection found in Casp1$^{-/-}$ mice was mainly due to the defective *Casp11* neighboring gene that was carried along as passenger mutation (Kayagaki et al., 2011). A later study could show that targeting of other *Casp11* neighboring genes, such as *Panx1*, also led to a resistance toward lethal LPS injection, if ESCs were derived from 129 mice, but not when B6-derived ESCs were used (Berghe et al., 2015). These two examples illustrate the potential impact of 129-derived passenger mutations and possible consequences, if they remain undetected.

P2X7 is a homotrimeric, adenosine triphosphate (ATP)-gated ion channel expressed on the cell surface of many immune cells (Bartlett et al., 2014). During tissue damage and inflammation ATP is released into the extracellular space where it serves as damage-associated molecule (DAMP). ATP-induced activation of P2X7 in macrophages and microglia triggers the formation of the NACHT-, LRR-, and

[1]Department of Neurology, University Medical Centre Hamburg-Eppendorf, 20246 Hamburg-Eppendorf, Germany

[2]IGF, Univ. Montpellier, CNRS, INSERM, 34094 Montpellier, France

[3]LabEx ICST, 34094 Montpellier, France

[4]Walther Straub Institute for Pharmacology and Toxicology, Ludwig-Maximilians-Universität München, 80336 Munich, Germany

[5]Institute of Neuroimmunology und Multiple Sclerosis (INIMS), University Medical Centre Hamburg-Eppendorf, 20246 Hamburg, Germany

[6]Institute of Immunology, University Medical Centre Hamburg-Eppendorf, 20246 Hamburg, Germany

[7]These authors contributed equally

[8]Senior authors

[9]Lead Contact

*Correspondence: b.rissiek@uke.de

https://doi.org/10.1016/j.isci.2020.101870

PYD-domain-containing protein 3 (NLRP3) inflammasome, consisting of NLRP3, the adaptor protein apoptosis-associated speck-like protein-containing CARD (ASC), and caspase 1. The NLRP3 inflammasome catalyzes the processing of pro-interleukin 1 beta (pro-IL-1β) into its active form IL-1β (Ferrari et al., 1997, 2006). In the mouse, certain T cell populations have been identified as "high P2X7" expressers: these are regulatory T cells (Treg) (Aswad et al., 2005; Hubert et al., 2010), cytotoxic lymphocytes (CTL) from the lamina propria (Heiss et al., 2008), natural killer T cells (NKT), follicular helper T cells (Tfh) (Proietti et al., 2014), and tissue-resident memory T cells (Trm) (Rissiek et al., 2018b). Autocrine ATP release followed by activation of P2X7 and other P2X receptors plays a role in various T cell functions, including in IL-2 secretion, metabolic fitness, and cell migration (da Silva et al., 2018; Ledderose et al., 2018; Rissiek et al., 2015; Schenk et al., 2008). High concentrations of ATP and prolonged activation of P2X7 on T cells, however, is a strong trigger of T cell death (Scheuplein et al., 2009). In contrast to human T cells, mouse T cells exhibit an alternative way of P2X7 activation, which is triggered by ecto-ADP-ribosyltransferase C2.2 (ARTC2.2). ARTC2.2 utilizes nicotinamide adenine dinucleotide (NAD^+), which is also released as DAMP during tissue damage, to ADP-ribosylate a variety of cell surface proteins such as CD25 (Teege et al., 2015), CD8β (Lischke et al., 2013), FcγR1, FcγR2b (Rissiek et al., 2017), and P2X7 (Seman et al., 2003). ADP-ribosylation of arginine 125 in the extracellular loop of P2X7 (Adriouch et al., 2008) acts like a covalently bound P2X7 agonist (Schwarz et al., 2009). Of note, 10-fold lower concentrations of NAD^+ compared with ATP are needed to activate T cell P2X7 receptors, and its ADP-ribosylation ultimately leads to NICD (Seman et al., 2003). Our own studies revealed that NAD^+ is also released during preparation of primary T cells from mouse organs such as spleen and lymph nodes (Rissiek et al., 2014; Scheuplein et al., 2009). Interestingly, ARTC2.2 is active at 4°C; however, ADP-ribosylation-mediated gating of P2X7 needs temperatures above 30°C (Scheuplein et al., 2009). This implicates that T cells prepared freshly on ice appear vital, but incubation at 37°C can trigger cell death in T cells that co-express high level of ARTC2.2 and P2X7 skewing the results of cytokine secretion assays as has been demonstrated for Trm, NKT, and Tfh (Borges da Silva et al., 2019; Georgiev et al., 2018; Rissiek et al., 2018b). The problem of P2X7 ADP-ribosylation during cell preparation can be solved by injecting an ARTC2.2-blocking nanobody (clone s+16a) into the mice 30 min before harvesting the mouse organs (Hubert et al., 2010; Koch-Nolte et al., 2007; Rissiek et al., 2014).

In the mouse, the *P2rx7* gene is located on chromosome 5 with 95 other characterized, protein-coding genes being within a distance of 2 megabases (Mb) upstream and downstream of *P2rx7* (Table S1). For *P2rx7*, a SNP (rs48804829) introduces a change of proline to leucine at amino acid position 451 in the cytosolic C-terminal tail of P2X7. The 129 and BALB/c mouse strains harbor the $P2X7^{451P}$ variant, whereas C57BL/6 (B6) mice express the loss-of-function $P2X7^{451L}$ variant. Studies revealed that $P2X7^{451P}$ and $P2X7^{451L}$ differ in their capacity to induce the formation of a P2X7-associated membrane pore (Adriouch et al., 2002) but not in P2X7-triggered calcium influx (Le Stunff et al., 2004; Sorge et al., 2012). No comparative P2X7 expression studies among mouse strains that express $P2X7^{451P}$ and $P2X7^{451L}$ have been performed. In this study, we analyzed P2X7 expression on T cell populations from different mouse strains. We show that CTL and helper T cells (Th) from strains that harbor $P2X7^{451P}$ express much higher P2X7 levels than cells derived from $P2X7^{451L}$ strains. As 129 mice express $P2X7^{451P}$ whereas B6 mice express $P2X7^{451L}$, we hypothesized that a 129-derived *P2rx7* gene could introduce an experimental bias when passed along as passenger mutation in congenic mice. Here, we demonstrate that in $P2rx4^{tm1Rass}$ mice Th and CTLs are much more prone to NICD compared with their wild-type (WT) counterparts. As consequence, these T cells appear less potent in terms of cytokine production and migration. However, when ARTC2.2 is blocked during cell preparation, the functional deficits of B6-P2X4ko T cells vanish. We identify other congenic mouse strains with targeted *P2rx7* neighboring genes that also carry the 129-derived *P2rx7* passenger mutation. Our study emphasizes the importance of checking the ESC origin of transgenic mice and analyzing them for passenger mutations in order to prevent misinterpretation of experimental results.

RESULTS

P2X7 Expression Levels on T cells in Laboratory Mouse Strains Are Associated with the P2X7 451P/L Polymorphism

The well-characterized SNP rs48804829 leads to a proline (451P) to leucine (451L) exchange at amino acid position 451 in the P2X7 protein. B6 mice express the $P2X7^{451L}$ variant, whereas 129 and BALB/c mice express the $P2X7^{451P}$ variant. This SNP affects P2X7 pore formation (Adriouch et al., 2002; Sorge et al., 2012). In order to determine whether this SNP is associated with P2X7 expression levels, we analyzed the RNA sequencing dataset provided by Mostafavi et al. to compare *P2rx7* mRNA expression levels of $CD4^+$ T cells from 23 different mouse strains (Mostafavi et al., 2014). The results show that 451P strains express

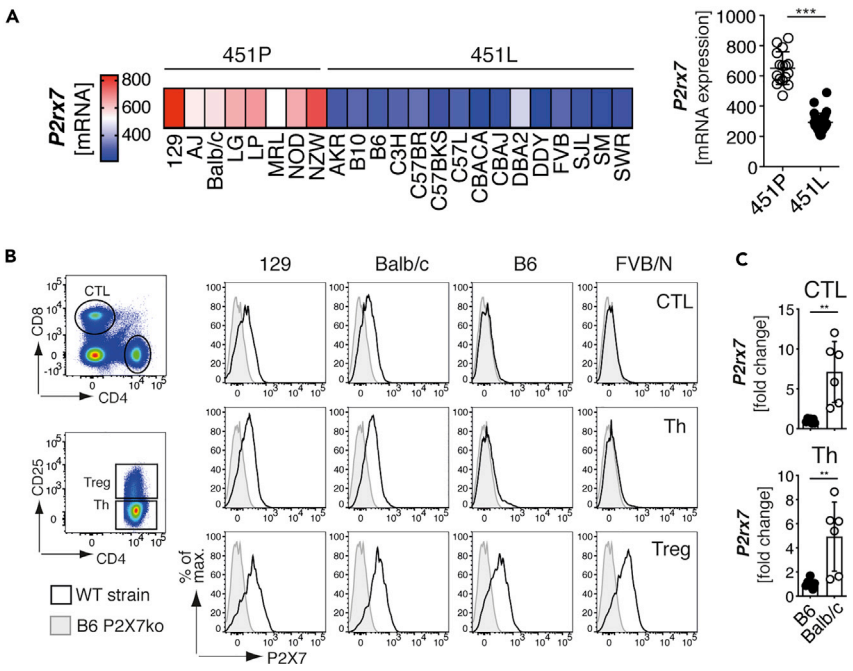

Figure 1. P2X7 Expression Levels in T cells Are Associated with the 451P/L Polymorphism

(A) Comparison of *P2rx7* mRNA expression on $CD4^+$ T cells from individual mouse strains expressing P2X7 451P (white) or 451L (black). *P2rx7* mRNA data were pool among 451L and 451P strains and compared. mRNA expression data were obtained from www.imgen.org (Heng et al., 2008; Mostafavi et al., 2014).

(B) Flow cytometric analyses of cell surface P2X7 expression on $CD8^+$ cytotoxic T cells (CTL), $CD4^+CD25^-$ helper T cells (Th) and $CD4^+CD25^+$ regulatory T cells (Treg) of 129, BALB/c, B6, and FVB/N mice.

(C) *P2rx7* mRNA expression was analyzed in CTL and Th from B6 and BALB/c mice (n = 5–6). Data are represented as mean +/−SD. Statistical comparison of two groups was performed by using the Student's t test ($p < 0.05$ = */$p < 0.01$ = **/$p < 0.001$ = ***, ns = no significant).

higher *P2rx7* levels in $CD4^+$ T cells, compared with 451L strains (Figure 1A). We next analyzed 129, BALB/c, B6, and FVB/N T cells for their P2X7 expression using the P2X7-specific monoclonal antibody Hano44 (Adriouch et al., 2005) and flow cytometry. In agreement with the RNA expression analysis, the results show higher cell surface levels of P2X7 on $CD8^+$ cytotoxic T lymphocytes (CTL) and $CD4^+$ helper T cells (Th) from 129 and BALB/c mice than from B6 and FVB/N mice (Figure 1B). Of note, regulatory T cells (Treg) display high levels of P2X7 on the cell surface in all analyzed mouse strains. Because naive and effector memory T cells were described to exhibit different P2X7 expression levels (Romagnani et al., 2020), we also analyzed P2X7 expression on naive ($CD62L^+CD44^{low}$) and effector/memory ($CD62L^-CD44^{high}$, TEM) $CD4^+$ T cells. Here, we could show that P2X7 expression was higher in naive $CD4^+$ T cells from 129 and BALB/c mice compared with B6 and FVB/N mice, whereas TEM from all analyzed strains expressed similarly high level of P2X7 (Figure S1). Comparison of *P2rx7* mRNA levels from CTL and Th cells of B6 and BALB/c mice confirmed that both BALB/c cell population expressed about 5-fold higher *P2rx7* mRNA levels (Figure 1C). Hence, our data show that the 451P/L *P2rx7* polymorphism is associated with higher/lower P2X7 expression in two major T cell populations.

$P2rx4^{tm1Rass}$ Mice Carry the 129-Originating *P2rx7* Gene as Passenger Mutation

One of the first P2X4-deficient mouse lines, $P2rx4^{tm1Rass}$, was generated by the Rassendren lab in 2006 (Sim et al., 2006). Here, *P2rx4* was targeted in ESCs of the 129 mouse strain and the generated P2X4ko mice were then backcrossed onto the B6 background. Because *P2rx4* and *P2rx7* are adjacent genes on mouse chromosome 5, we hypothesized that the 129-derived $P2X7^{451P}$ is still present in B6-P2X4ko mice (Figure 2A). We confirmed this hypothesis by sequencing an amplified fragment flanking rs48804829 (Figure 2B). B6-WT and B6-P2X4ko thus differ in both *P2rx4* and *P2rx7*. In order to obtain mice that differ only in *P2rx4* but not *P2rx7*, we backcrossed P2X4ko mice onto the BALB/c background for 13 generations. This way, we obtained Balb/c-WT and Balb/c-P2X4ko mice, which both express $P2X7^{451P}$ in addition to B6-WT and

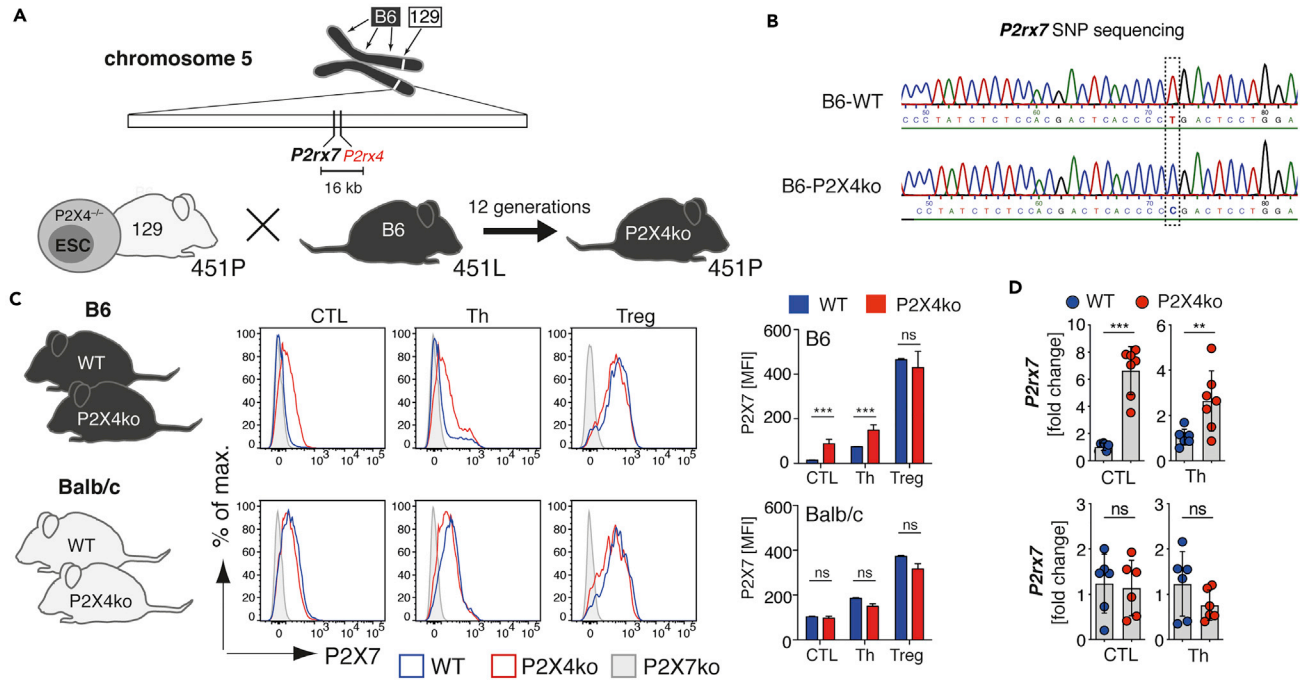

Figure 2. P2X4ko Mice Harbor a *P2rx7* Passenger Mutation

(A) *P2rx7* and *P2rx4* are neighboring genes on mouse chromosome 5. A non-synonymous SNP in the *P2rx7* gene introduces a single amino acid change in the P2X7 protein: 129 mice express a proline at position 451 (451P), whereas B6 mice express a leucine at position 451 (451L). P2X4ko mice were generated by deleting exon 1 of *P2rx4* in embryonic stem cells derived from a 129 mouse strain. These mice express the 451P variant of P2X7. Backcrossing of P2X4ko onto the B6 background leads to the generation of B6-P2X4ko mice that express the 451P variant, due to a high degree of genetic linkage.

(B) Sequencing of cDNA obtained from isolated immune cell mRNA confirmed the 451P passenger mutation in the B6-P2X4ko mice.

(C) Flow cytometric analyses of cell surface P2X7 expression on CTL, Th, and Treg of WT and P2X4ko mice on the B6 and BALB/c background. The mean fluorescence intensity (MFI) of P2X7 on the different T cell populations from WT and P2X4ko mice (n = 3) was compared.

(D) *P2rx7* mRNA of FACS-sorted WT and P2X4ko CTL, Th, and Treg (B6 and BALB/c) was analyzed (n = 6–7). Data are represented as mean +/−SD. Statistical comparison of two groups was performed by using the Student's t test ($p < 0.05$ = */$p < 0.01$ = **/$p < 0.001$ = ***, ns = no significant).

B6-P2X4ko mice that express $P2X7^{451L}$ and $P2X7^{451P}$. We next compared P2X7 expression on T cells of B6 and BALB/c P2X4ko mice and the corresponding WT strains. Here, we observed that CTL and Th, but not Treg, from B6-P2X4ko mice expressed higher level of P2X7 when compared with B6-WT T cells (Figure 2C). Again, when separating naive $CD4^+$ Th and $CD4^+$ TEM, P2X7 expression was higher in naive $CD4^+$ T cells from B6-P2X4ko mice compared with B6-WT mice, and TEM from both strains expressed comparable level of P2X7 (Figure S2A). Further, BALB/c P2X4ko and WT T cells exhibited comparable P2X7 expression levels (Figure 2C). Finally, we isolated mRNA from CTL and Th from all four strains and analyzed *P2rx7* mRNA expression. The results show that B6-P2X4ko CTL and Th express 3- to 6-fold higher level of *P2rx7* mRNA compared with B6-WT T cells. There was no statistically significant difference in *P2rx7* mRNA expression in BALB/c P2X4ko and WT CTL and Th (Figure 2D). Of note, frequencies of T cells in blood, lymph nodes, and spleen were similar in B6-WT and P2X4ko mice and Balb/c-WT and Balb/c-P2X4ko mice, with a slight but significantly reduced frequency of CTLs in lymph nodes and spleen of B6-P2X4ko mice (Figure S2B). Taken together, B6-P2X4ko mice carry the $P2X7^{451P}$ variant as passenger mutation, which is associated with a higher P2X7 expression on T cells compared with corresponding WT cells.

B6-P2X4ko T Cells Are More Sensitive to ATP and NAD^+ Compared with B6-WT T Cells

P2X7 expression levels likely influence the cellular response to adenosine triphosphate (ATP). To analyze this, we generated stably transfected HEK cell lines that express $P2X7^{451L}$ or $P2X7^{451P}$, each in the two major splice variants (the canonical P2X7a and P2X7k) (Nicke et al., 2009; Schwarz et al., 2012). We first compared ATP-induced calcium responses of these variants by real-time flow cytometry. $P2X7k^{451L}$ HEK cells were labeled with $eFluor^{450}$ and mixed with unlabeled $P2X7k^{451P}$ HEK cells. Mixed cells were loaded with Fluo4 and were analyzed in parallel. In order to adjust for cell surface levels of P2X7, cells were stained

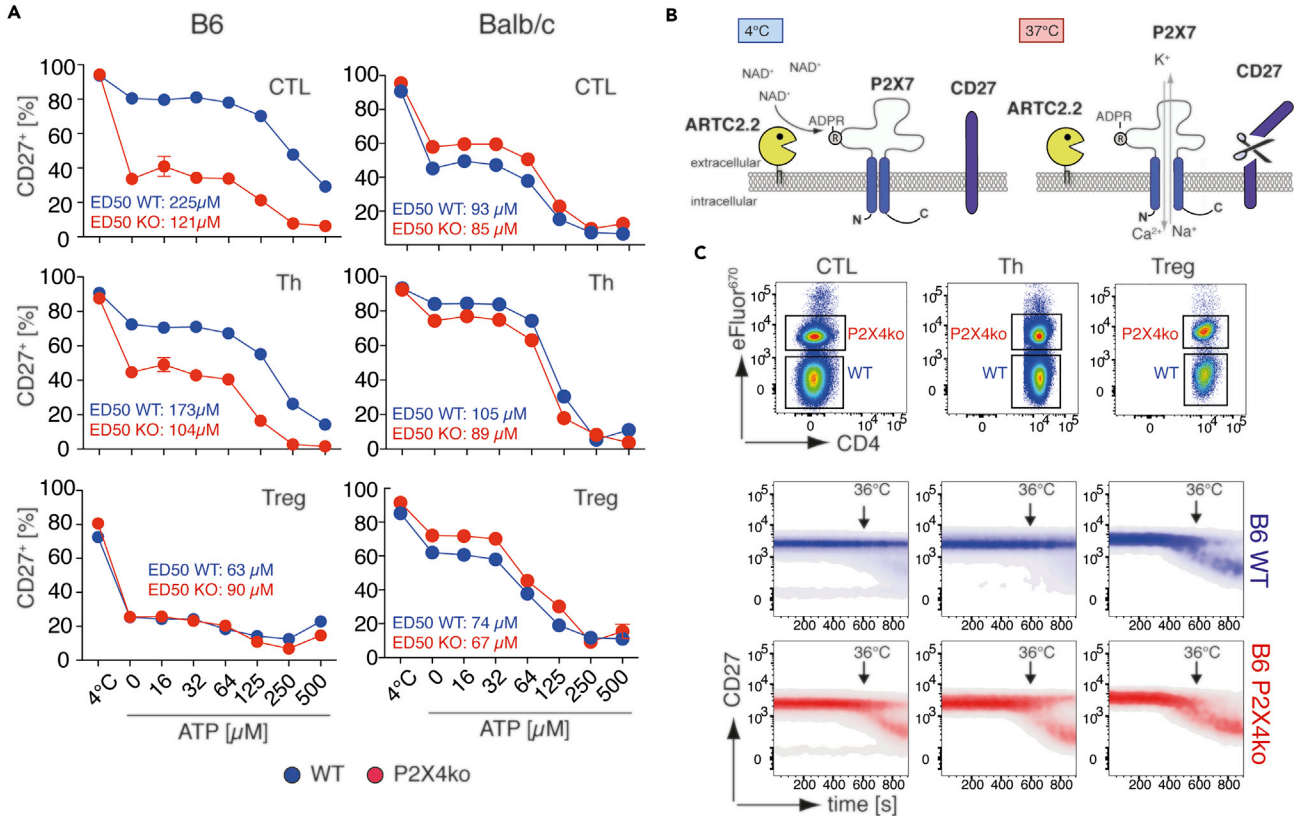

Figure 3. B6 P2X4ko T cells Show an Increased Response to ATP and NAD$^+$-mediated P2X7 Activation When Compared with B6 WT T cells

(A) CTL, Th, and Tregs from WT (blue) and P2X4ko mice (red) on the B6 and BALB/c background were incubated at 37°C in the presence of 0–500 μM ATP or left at 4°C. CD27 shedding was assessed as surrogate readout for P2X7 activation. ED50 for ATP stimulation was calculated.

(B) Ecto-ADP-ribosyltransferase ARTC2.2 can ADP-ribosylate P2X7 at arginine (R) 125. Extracellular NAD$^+$, which is released during cell preparation, can serve as substrate for ARTC2.2, even if cells are prepared at 4°C. Bringing the cells back to 37°C triggers gating of P2X7 inducing shedding of CD27.

(C) B6 P2X4ko splenocytes were labeled with eFluor^{670} and mixed with unlabeled B6 WT splenocytes. Mixed cells were stained with anti-CD27, and cell surface CD27 was monitored over time on CTL, Th, and Treg while increasing the temperature up to 36°C.

with AF647-conjugated Hano44 and the analysis gate was adjusted on the basis of P2X7 mean fluorescence intensity (MFI). All cell lines responded with a comparably strong and ATP dose-dependent Ca^{2+} influx (Figure S3A). Shifting the analysis gates in P2X7^{451L} HEK cells toward a higher P2X7 MFI and that in P2X7^{451P} HEK cells toward a lower P2X7 MFI resulted in increased and decreased calcium signals, respectively (Figure S3B). This suggests that the level of cell surface P2X7 influences ATP-induced calcium signals and likely also downstream functions. Because CTL and Th cells from B6-P2X4ko mice exhibit higher P2X7 expression levels, it is likely that they also react more sensitive to stimulation with ATP. To test this hypothesis, we incubated splenocytes from B6-WT and B6-P2X4ko mice with rising concentrations of ATP for 10 min at 37°C and measured the loss of CD27 from the cell surface, a well-known readout for P2X7 activation on T cells (Rissiek et al., 2018a). Strikingly, the majority of B6-P2X4ko CTL and Th responded already to incubation at 37°C with a massive loss of CD27 from their cell surface, in contrast to their B6-WT counterparts (Figure 3A). In contrast, Treg cells from B6-WT and B6-P2X4ko mice both responded with a strong loss of CD27, when incubated at 37°C. Likewise, B6-P2X4ko CTL and Th were more sensitive to addition of exogenous ATP, with an ED_{50} of 120μM (P2X4ko) and 225μM (WT) for CTL and 100μM (P2X4ko) and 170μM (WT) for Th cells. Of note, a similar experiment with BALB/c P2X4ko and BALB/c WT splenocytes showed no significant difference in ATP sensitivity between P2X4ko and WT T cells.

The loss of CD27 during incubation at 37°C is most likely due to activation of P2X7 by ADP-ribosylation in response to extracellular NAD$^+$ released during cell isolation (Figure 3B). This effect has been well described for Treg, natural killer T cells (NKTs), tissue-resident memory T cells (Trm), and T follicular helper cells (Georgiev et al., 2018; Rissiek et al, 2014, 2018b; Scheuplein et al., 2009), which co-express P2X7 and

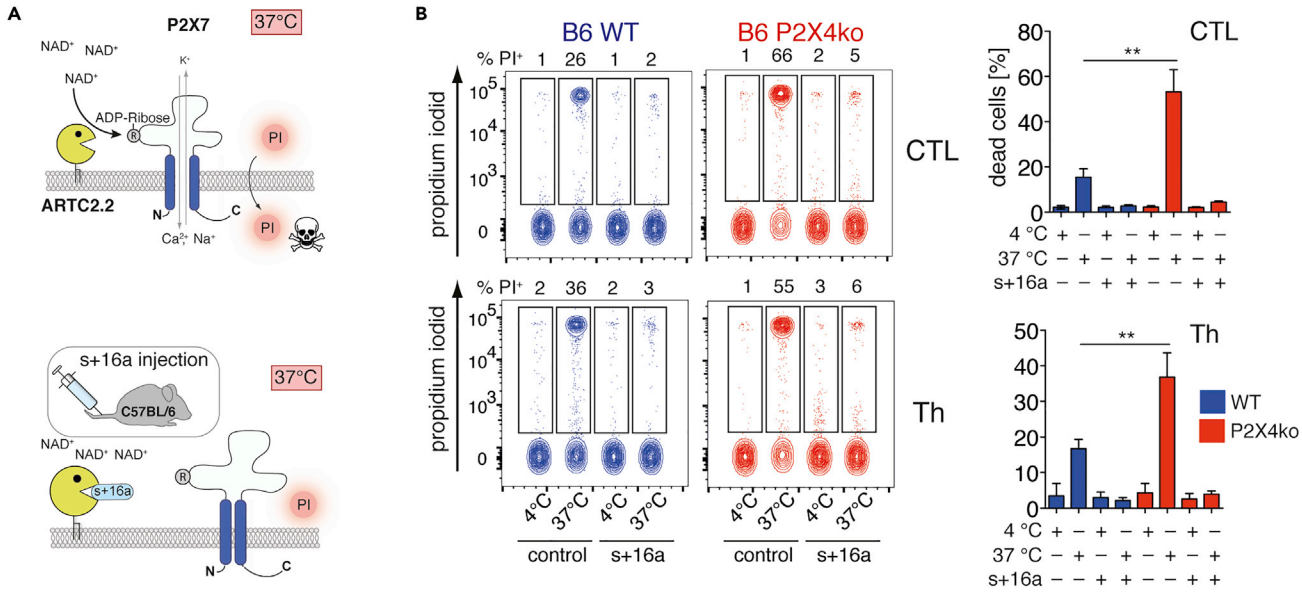

Figure 4. B6-P2X4ko T cells Exhibit Enhanced NICD

(A) B6 WT and B6 P2X4ko mice were injected or not with anti-ARTC2.2 nanobody s+16a in order to prevent P2X7 ADP-ribosylation during cell preparation. (B) CTL and Th from spleen were FACS sorted, and obtained cells were incubated at 37°C for 2 h or left at 4°C. Cell vitality was measured by propidium iodide (PI) uptake (n = 3). Data are represented as mean +/−SD. Statistical comparison of two groups was performed by using the Student's t test ($p < 0.05$ = */$p < 0.01$ = **/$p < 0.001$ = ***, ns = no significant).

ARTC2.2 (Glowacki et al., 2002). Although ADP-ribosylation usually occurs at 4°C, ADP-ribosylation-induced gating of P2X7, however, needs temperatures above 30°C (Scheuplein et al., 2009). To better visualize the temperature dependence of this process, we labeled B6-P2X4ko splenocytes with eFluor^{670}, mixed them with unlabeled B6-WT splenocytes at 4°C, and then monitored the loss of CD27 on CTL, Th, and Treg cells at elevating temperatures using real-time flow cytometry. During the measurement, the sample was brought to 36°C while the CD27 signal was continuously monitored. Once the cells reached temperatures close to 36°C, the CD27 signal decreased in a fraction of cells (Figure 3C). Apparently, this loss of CD27 was more prominent in CTL and Th from B6-P2X4ko compared with corresponding B6-WT cells (Figure 3C). Again, Tregs from both B6-P2X4ko and B6-WT mice reacted with a pronounced loss of CD27 in this experimental setup. Of note, ARTC2.2 expression levels were comparable among individual T cell populations from P2X4ko and corresponding WT mice (Figure S4), as determined by flow cytometry.

The Increased Sensitivity of B6-P2X4ko T cells toward NICD Confounds Results from Functional Assays

The ultimate consequence of ADP-ribosylation-mediated P2X7 activation is NICD (Seman et al., 2003). Cell-preparation-related ADP-ribosylation of P2X7 on T cells can be prevented by injecting the ARTC2.2 blocking nanobody s+16a prior to sacrificing the mice (Figure 4A) (Koch-Nolte et al., 2007; Rissiek et al., 2014). Because CTL and Th from B6-P2X4ko mice are sensitive to P2X7-induced CD27 shedding at 37°C, we next tested whether this also results in an increased susceptibility toward NICD of FACS-sorted CTL and Th from mice that had been treated or not with s+16a. As a readout for cell death, we measured staining of cells with propidium iodide (PI). We observed that only a minor fraction of B6-WT CTL and Th (20%–30%) underwent NICD (Figure 4B). In contrast, 40%–60% of B6-P2X4ko CTL and Th were PI$^+$ after 2 h of incubation at 37°C. Of note, injection of s+16a prevented NICD of B6-WT and B6-P2X4ko CT and Th.

Next, we compared cytokine production and migration of CTL and Th from mice that had been treated or not with s+16a. For cytokine analyses, we stimulated FACS-sorted CTL with phorbole-12-myristate-13-acetate (PMA)/ionomycin. When comparing CTL from untreated B6-P2X4ko and B6-WT mice, it appeared that P2X4-deficiency dampened secretion of IL-2, IFNγ, and TNFα. However, when ADP-ribosylation during cell preparation was prevented by s+16a injection, CTL from both mouse lines produced comparable amounts of all three cytokines (Figure 5A). Because P2X4 has been attributed a role in T cell migration

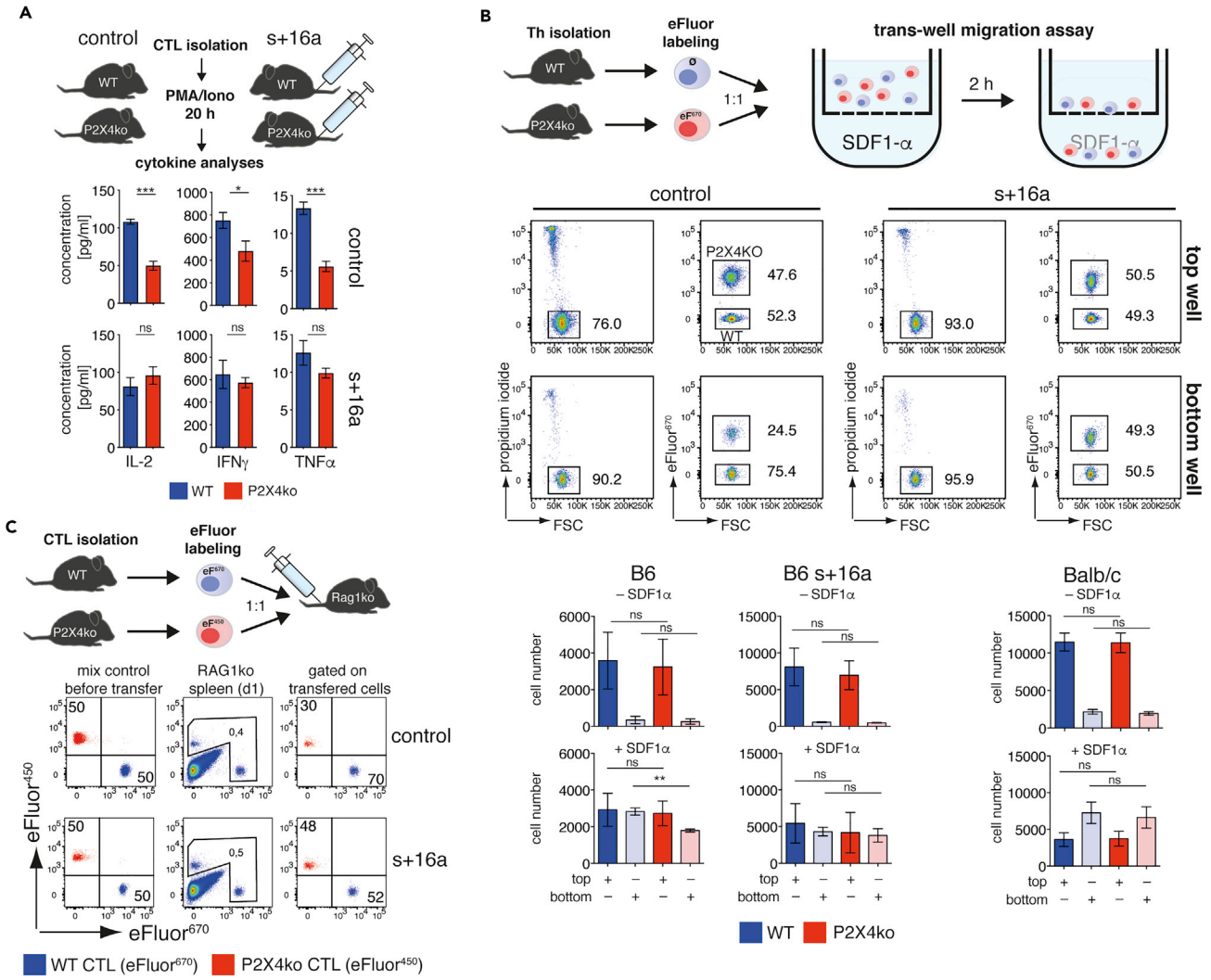

Figure 5. The enhanced NICD of B6-P2X4ko T cells Can Lead to Misinterpretation of Functional Assays

(A) B6 WT and P2X4ko mice were injected (s+16a) or not (control) with anti-ARTC2.2 nanobody s+16a. 5 × 10^4 CTL were FACS sorted and stimulated *ex vivo* with PMA/ionomycin for 20 h. IL-2, IFNγ, and TNFα in the supernatants were measured by cytometric bead array.

(B) 1 × 10^5 eFluor^{670} labeled Th from P2X4ko mice (B6, B6 treated with s+16a or BALB/c) and 1 × 10^5 unlabeled Th from corresponding WT mice were mixed and transferred to the top well of a transwell chamber in order to perform a comparative migration assay toward SDF1α, which was used as chemoattractant in the bottom well. Number of vital (PI–) Th in top and both wells was determined after 2 h of incubation at 37°C.

(C) Comparative adoptive transfer of CTL obtained from B6 WT and P2X4ko mice that have been treated or not with s+16a was performed. Cells were differentially labeled with eFluor^{670} and eFluor^{450}, and 4 × 10^5 cells mixed in a 1:1 ratio were i.v. injected into RAG1ko mice. Spleens were analyzed after 24 h for the presence of transferred mixed cells.

Data are represented as mean +/−SD. Statistical comparison of two groups was performed by using the Student's t test ($p < 0.05$ = */$p < 0.01$ = **/$p < 0.001$ = ***, ns = no significant).

(Ledderose et al., 2018), we next compared B6 WT and P2X4ko Th in an *in vitro* migration assay using a trans-well chamber and SDF1α (CXCL12) as chemoattractant in the bottom chamber. In order to compare WT and P2X4ko Th side by side, we labeled P2X4ko Th with eFluor^{450}, mixed them with unlabeled WT Th, and measured the ratio of vital (PI-negative) cells in the top and bottom well (Figure 5B). The presence of SDF1α markedly increased the migration of Th cells from the top to the bottom wells; however, B6-P2X4ko Th cells seemed to migrate less compared with B6-WT Th (Figure 5B). This difference in migration was not observed with cells from mice that had been treated with the ARTC2.2-blocking nanobody s+16a. This suggests that increased NICD susceptibility rather than a P2X4-mediated effect on migratory capacity causes the difference in Th migration. This conclusion is supported by the finding that WT and P2X4ko Th cells

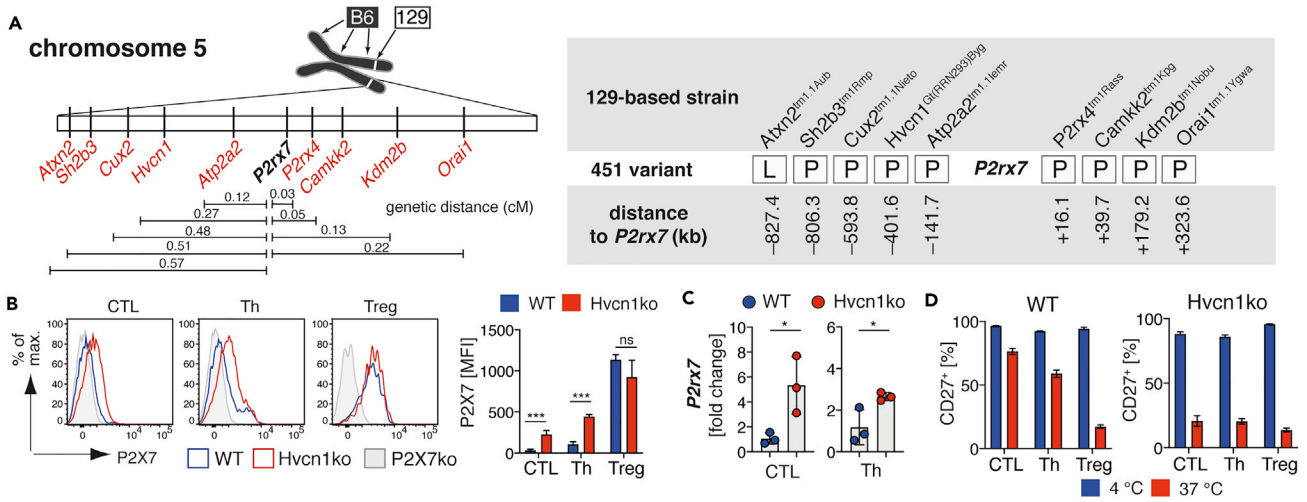

Figure 6. The 129-derived *P2rx7* Passenger Mutation Is Present in Other Transgenic Mouse Strains

(A) Nine congenic mouse strains with targeted genes in close proximity of *P2rx7* were analyzed for the presence of the SNP leading to the 451P/L polymorphism.

(B) P2X7 expression was determined on CTL, Th, and Treg from B6-Hvcn1ko carrying the 129-derived P2rx7 passenger mutation (n = 3).

(C) *P2rx7* mRNA expression was analyzed in CTL and Th from B6-Hvcn1ko and B6-WT mice.

(D) CTL, Th, and Treg from Hvcn1ko and B6-WT were incubated at 4°C and 37°C for 15 min in order to measure the impact of P2X7 ADP-ribosylation by shedding of CD27. Data are represented as mean +/−SD. Statistical comparison of two groups was performed by using the Student's t test ($p < 0.05$ = */$p < 0.01$ = **/$p < 0.001$ = ***, ns = no significant).

from BALB/c mice, which do not differ in NICD susceptibility, also did not differ in their migration capacity toward SDF1α (Figure 5B). Finally, we performed *in vivo* adoptive transfer experiments where we mixed differentially labeled B6-WT and B6-P2X4ko CTL harvested from mice that had been treated or not with s+16a in a 1:1 ratio and transferred them into RAG1ko mice. Twenty-four hours after adoptive transfer, spleens of the injected RAG1ko mice were analyzed for the presence of the injected CTLs. Here, we retrieved about 2-fold more B6-WT than B6-P2X4ko CTL from the RAG1ko spleens, again suggesting a deficit in migration capacity of the B6-P2X4ko CTL (Figure 5C). However, when B6-WT and B6-P2X4ko CTL were harvested from s+16a treated mice, B6-WT and B6-P2X4ko CTL were retrieved at a ratio of almost 1:1. The results with these three functional assays demonstrate increased P2X7 expression rather than loss of P2X4 alters several functions of Th and CTL on the B6 background.

The *P2rx7* Passenger Mutation Can Be Found in Other Transgenic Mice

A genetic distance of 2 Mb in the mouse genome is, on average, equivalent to 1 centiMorgan (cM) (Bryant et al., 2018). This implicates that for 129-derived transgenic mice genes in a 2 Mb maximum distance of the targeted gene are retained with a theoretical probability of 90% after 10 generations of backcrossing. *P2rx4* is with a distance of only 16 kb the nearest neighbor gene of *P2rx7*. However, there are 94 other characterized, protein-coding genes within 2 megabases (Mb) upstream and downstream of *P2rx7*. A search in the Mouse Genome Informatics (MGI) database resulted in 96 mouse strains generated from 129-derived ESCs in which genes within +/−2MB of *P2rx7* had been targeted (Table S1). To test our hypothesis that the *P2rx7* passenger mutation will affect T cell functions in mice of targeted neighboring genes, we analyzed nine other mouse strains with targeted *P2rx7* neighboring genes on the B6 background for the presence of the 129-derived *P2rx7* passenger mutation. Results of the SNP rs48804829 sequencing revealed that eight of the nine analyzed strains harbor the 129-derived *P2rx7* passenger mutation (Figure 6A). Only in the Atxn2$^{tm1.1Aub}$ mouse strain the 129-derived P2X7^{451P} was exchanged by the B6-derived P2X7^{451L}. In order to reproduce the phenotypical and functional consequences of the *P2rx7* passenger mutation described for P2rx4^{tm1Rass}, we evaluated T cells from B6-Hvcn1$^{Gt(RRRN293)Byg}$ (B6-Hvcn1ko) mice for the expression of P2X7. Here, we obtained a similar result as for P2rx4^{tm1Rass}: the P2X7 cell surface expression was significantly higher on B6-Hvcn1ko CTL and Th compared with B6-WT (Figure 6B). Similarly, *P2rx7* mRNA levels were increased in B6-Hvcn1ko CTL and Th in comparison to B6-WT CTL and Th (Figure 6C). As a consequence, B6-Hvcn1ko CTL and Th responded more pronounced to preparation-related P2X7

ADP-ribosylation, as indicated by a massive shedding of CD27 upon incubation at 37°C, when compared with B6-WT T cells (Figure 6D).

DISCUSSION

Passenger mutations are a phenomenon occurring in genetically modified mice when the genetic background of the used ES cells and the genetic background of the line in which the modified gene was backcrossed are not identical. Even after backcrossing for more than 12 generations, the flanking regions of the modified gene often contain multiple foreign genes of ES cell origin, some of which can be differentially expressed between the transgenic strain and the supposed WT strain. Further, functionally inactive 129-derived passenger genes can introduce an experimental bias, as in the example of the Caspase-1 knockout mouse (Casp1^{tm1Flvw}). Here, the 129-derived ES cells used to generate Casp1^{tm1Flvw} (Kuida et al., 1995) introduced a defective *Casp11* gene in close proximity of the knocked out *Casp1* gene, thereby transferring resistance to otherwise lethal LPS injection to Casp1^{tm1Flvw} mice. The role of the inactive *Casp11* passenger gene in LPS resistance was unnoticed for more than 15 years until Kayagaki and colleagues revealed this important fact (Kayagaki et al., 2011). The defective *Casp11* gene was also found in other transgenic mice generated with 129-derived ES cells, such as Panx1$^{tm1.1Vshe}$ (Dvoriantchikova et al., 2012), again conferring these transgenic mice resistance to LPS (Berghe et al., 2015). These examples illustrate the importance of screening transgenic mice with a congenic background for passenger mutations in order to avoid experimental bias.

In this study we demonstrate that the expression of P2X7 on conventional helper T cells as well as on cytotoxic T cells differs among laboratory mouse strains. Interestingly, P2X7 expression was high on T cells from strains carrying the 451P variant of P2X7, whereas P2X7 expression was low on T cells from strains carrying the 451L variant resulting from the SNP rs48804829. Despite the clear correlation between the rs48804829 SNP and *P2rx7* expression levels in T cells, it appears unlikely that the rs48804829 SNP alone is responsible for the difference in P2X7 expression levels. According to the Wellcome Sanger Institute SNP database, there are 172 SNPs within the *P2rx7* gene (+/− 1 kbp), which differ in B6 and 129 mice (including the rs48804829 SNP). Further, 129 mice harbor a 249 bp intronic deletion close to exon 12 of *P2rx7* (Keane et al., 2011). Both SNPs and the deletion could affect accessibility of the *P2rx7* locus or the binding of certain transcription factors. Therefore, the reason(s) for higher *P2rx7* expression in CD4 and CD8 T cells in 129 mice compared with B6 remain to be determined.

Regarding T cells, the 451L P2X7 variant of B6 mice is often referred to as less sensitive or loss-of-function variant, compared with the e.g. the BALB/c 451P P2X7 variant (Bartlett et al., 2014; de Campos et al., 2012; Proietti et al., 2014). However, the lower cell surface levels of P2X7 on B6 T cells compared with BALB/c T cells also contribute to the reduced ATP/NAD$^+$ sensitivity. This is underlined by our findings with P2X7-transfected HEK cells, which show comparable ATP-induced calcium influx of 451L and 451P variants when adjusted for P2X7 expression levels.

Because T cells from 129 mice (451P) and B6 mice (451L) mice differ in their P2X7 expression level, we hypothesized that this difference would be passed on as passenger mutation to the B6 background from 129-based mice with targeted genes in the *P2rx7* genetic neighborhood. For B6 mice in which the nearest neighbor gene of *P2rx7*, *P2rx4*, had been targeted in 129 ES cells, we found that these B6 P2X4ko mice (1) carry *P2rx7* 451P as passenger gene, (2) express higher levels of P2X7 on CD4 and CD8 T cells, when compared with B6 WT, (3) are more sensitive to treatment with exogenous ATP and NAD$^+$, and (4) are more prone to ADP-ribosylation of P2X7 during cell preparation, resulting in NAD-induced cell death (NICD) in a higher fraction of cells compared with B6 WT. Increased sensitivity of NICD is receiving more and more attention, because important T cell populations that co-express high level of P2X7 and ARTC2.2, such as Tregs, NKTs, Tfh, and Trm, are highly affected by ADP-ribosylation during cell preparation (Georgiev et al., 2018; Hubert et al., 2010; Proietti et al., 2014; Rissiek et al, 2014, 2018b; Stark et al., 2018). The analyses and functional characterization of these cell populations has been greatly improved by the use of the ARTC2.2-blocking nanobody s+16a, which prevents ADP-ribosylation of P2X7 during cell preparation and preserves the vitality of the prepared cells in functional assays and during adoptive transfer (Koch-Nolte et al., 2007; Rissiek et al., 2014). Similarly, injection of s+16a into P2X4ko mice preserved the vitality of the NAD-sensitive P2X4ko T cells. Otherwise, the higher loss of P2X4ko T cells during functional assays *in vivo* and *in vitro*, due to NICD, skews experimental results, as demonstrated by our cytokine expression and migration analyses. This likely holds also for previously reported studies with

T cells from P2rx4^{tm1Rass} mice, e.g. where polyclonally activated P2X4ko T cells exhibited less proliferation and granzyme B expression compared with T cells from B6 WT mice (Ventre et al., 2017).

We found that eight of nine other congenic strains on the B6 background derived from 129 ES cells with targeted genes in the *P2rx7* neighborhood carried the 129-derived *P2rx7* passenger gene. We had further access to one of these strains, B6-Hvcn1$^{Gt(RRRN293)Byg}$ mice, and were able to reproduce the phenotype of P2rx4^{tm1Rass} T cells, suggesting that our findings can be extrapolated to other congenic mice carrying the *P2rx7* passenger gene. *Orai1*, for example, plays an important role in T cell function (Nohara et al., 2015) and is also a neighboring gene of *P2rx7*. Studies have demonstrated that genetic ablation of *Orai1* in mice on a pure B6 background, e.g. Orai1^{tm1Rao} or Orai1^{tm1Fesk}, leads to a diminished T cell cytokine production (Kim et al., 2014; McCarl et al., 2010), underlining the importance of *Orai1* in T cell function. In our study, we could identify the 451P *P2rx7* passenger mutation in the 129-derived Orai1$^{tm1.1Ygwa}$ strain. These mice were used in a study to generate T-cell-specific B6 Orai1ko mice by crossing them with CD4-Cre mice. Interestingly, CD8 T cells from these T-cell-specific B6-Orai1ko were less potent in killing peptide-loaded EL-4 tumor cells *in vitro* compared with CD8 T cells from B6-WT mice (Kim et al., 2017). Further, T cells from the 129-based Orai1$^{Gt(XL922)Byg}$ mouse also exhibited reduced IL-2 and IFNγ production in response to polyclonal T cell receptor stimulation (Vig et al., 2008). It is conceivable that these mice also harbor the 129-derived *P2rx7* passenger gene, and their T cells are consequently also more sensitive to NICD than the WT controls. It would be interesting to determine whether treatment with the ARTC2.2 blocking nanobody s+16a has any impact on the outcome of these experimental settings.

Further, it is worth noting that when working with conditional knockouts, the control group can have a great impact on the results and interpretation when it comes to the impact of passenger mutations: a comparison of Cre – floxed and Cre + floxed mice would "silence" the impact of a passenger mutation, because it is present in both mice. In contrast, a comparison of Cre + floxed and Cre + WT or pure WT mice can introduce an experimental bias triggered by a passenger mutation.

In conclusion, our results emphasize the importance of a thorough analysis of the genetic neighborhood of 129-based transgenic mice on the B6 background. As demonstrated for P2rx4^{tm1Rass}, a passenger mutation in the neighboring *P2rx7* gene can introduce an experimental bias. Apart from T cells, which were the focus of this study, it would be worthwhile to evaluate the impact of the *P2rx7* passenger mutation on other P2X7 expressing cell populations such as astrocytes, neurons, or adipocytes.

Limitations of the Study

Our work clearly demonstrates the impact of the *P2rx7* passenger mutation on the vitality of T cell from B6-P2X4ko mice. However, one has to keep in mind that a transgenic strain in one animal facility can carry a certain passenger mutation, whereas the same strain bred in another animal facility might have successfully replaced the passenger mutation during backcrossing. Therefore, it is highly recommended to check for possible passenger mutations when working with newly imported mouse strains in order to avoid experimental bias.

Resource Availability

Lead Contact

Further information and requests for resources and reagents should be directed to and will be fulfilled by the Lead Contact, Björn Rissiek (b.rissiek@uke.de).

Materials Availability

This study did not generate new unique reagents.

Data and Code Availability

This study did not generate/analyze datasets/code.

METHODS

All methods can be found in the accompanying Transparent Methods supplemental file.

SUPPLEMENTAL INFORMATION

Supplemental Information can be found online at https://doi.org/10.1016/j.isci.2020.101870.

ACKNOWLEDGMENTS

The authors would like to thank the following colleagues for providing genomic DNA samples of transgenic mice: Georg Auburger(Atxn2$^{tm1.1Aub}$), Satoshi Takaki and Meena S Madhur (Sh2b3^{tm1Rmp}), Marta Nieto and Elia Marcos Grañeda (Cux2$^{tm1.1Nieto}$), Carmella Evans-Molina (Atp2a2$^{tm1.1Iemr}$), David Carling (Camkk2^{tm1Kpg}), Nobuaki Yoshida and Manabu Ozawa (Kdm2b^{tm1Nobu}), and Yousang Gwack (Orai1$^{tm1.1Ygwa}$). The authors would like to thank the HEXT FACS Core Facility (Hamburg, Germany) for cell sorting. This work was funded by the Deutsche Forschungsgemeinschaft (DFG, German Research Foundation–Project-ID: 335447717—SFB1328, A06 and A16 to MAF, A10 and Z02 to FK-N, A13 to TM, and A15 to AN), the ''Hermann und Lilly Schilling-Stiftung für Medizinische Forschung'' to TM, and a faculty grant to BR (FFM, NWF-17/07).

AUTHORS CONTRIBUTIONS

BR and ME-L performed all experiments and analyzed and interpreted the data. YD generated P2X7 stably transfected HEK cells. FR, LU, FU, and MAF provided essential material. AN, FK-N, and TM supervised the experiments and assisted with data interpretation and manuscript preparation. BR assembled the figures and wrote the manuscript, which has been reviewed by all authors.

DECLARATION OF INTERESTS

FK-N receives royalties from sales of antibodies developed in the lab via MediGate GmbH, a 100% subsidiary of the University Medical Center, Hamburg. All other authors declare no competing interests.

Received: July 13, 2020
Revised: October 26, 2020
Accepted: November 23, 2020
Published: December 18, 2020

REFERENCES

Adriouch, S., Bannas, P., Schwarz, N., Fliegert, R., Guse, A.H., Seman, M., Haag, F., and Koch-Nolte, F. (2008). ADP-ribosylation at R125 gates the P2X7 ion channel by presenting a covalent ligand to its nucleotide binding site. FASEB J. *22*, 861–869.

Adriouch, S., Dox, C., Welge, V., Seman, M., Koch-Nolte, F., and Haag, F. (2002). Cutting edge: a natural P451L mutation in the cytoplasmic domain impairs the function of the mouse P2X7 receptor. J. Immunol. *169*, 4108–4112.

Adriouch, S., Dubberke, G., Diessenbacher, P., Rassendren, F., Seman, M., Haag, F., and Koch-Nolte, F. (2005). Probing the expression and function of the P2X7 purinoceptor with antibodies raised by genetic immunization. Cell Immunol. *236*, 72–77.

Aswad, F., Kawamura, H., and Dennert, G. (2005). High sensitivity of CD4+CD25+ regulatory T cells to extracellular metabolites nicotinamide adenine dinucleotide and ATP: a role for P2X7 receptors. J. Immunol. *175*, 3075–3083.

Bartlett, R., Stokes, L., and Sluyter, R. (2014). The P2X7 receptor channel: recent developments and the use of P2X7 antagonists in models of disease. Pharmacol. Rev. *66*, 638–675.

Berghe, T.V., Hulpiau, P., Martens, L., Vandenbroucke, R.E., Van Wonterghem, E., Perry, S.W., Bruggeman, I., Divert, T., Choi, S.M., Vuylsteke, M., et al. (2015). Passenger mutations confound interpretation of all genetically modified congenic mice. Immunity *43*, 200–209.

Borges da Silva, H., Wang, H., Qian, L.J., Hogquist, K.A., and Jameson, S.C. (2019). ARTC2.2/P2RX7 signaling during cell isolation distorts function and quantification of tissue-resident CD8+ T cell and invariant NKT subsets. J. Immunol. *202*, ji1801613–j1802163.

Bryant, C.D., Ferris, M.T., De Villena, F.P.M., Damaj, M.I., Kumar, V., and Mulligan, M.K. (2018). Reduced complexity cross design for behavioral genetics. In Molecular-Genetic and Statistical Techniques for Behavioral and Neural Research, R.T. Gerlai, ed. (Elsevier), pp. 165–190.

da Silva, H.B., Beura, L.K., Wang, H., Hanse, E.A., Gore, R., Scott, M.C., Walsh, D.A., Block, K.E., Fonseca, R., Yan, Y., et al. (2018). The purinergic receptor P2RX7 directs metabolic fitness of long-lived memory CD8 + T cells. Nature *5*, 1.

de Campos, N.E., Marques-da-Silva, C., Corrêa, G., Castelo-Branco, M.T.L., de Souza, H.S.P., and Coutinho-Silva, R. (2012). Characterizing the presence and sensitivity of the P2X7 receptor in different compartments of the gut. J. Innate Immun. *4*, 529–541.

Dvoriantchikova, G., Ivanov, D., Barakat, D., Grinberg, A., Wen, R., Slepak, V.Z., and Shestopalov, V.I. (2012). Genetic ablation of Pannexin1 protects retinal neurons from ischemic injury. PLoS One *7*, e31991.

Ferrari, D., Chiozzi, P., Falzoni, S., Hanau, S., and Di Virgilio, F. (1997). Purinergic modulation of interleukin-1β release from microglial cells stimulated with bacterial endotoxin. J. Exp. Med. *185*, 579–582.

Ferrari, D., Pizzirani, C., Adinolfi, E., Lemoli, R.M., Curti, A., Idzko, M., Panther, E., and Di Virgilio, F. (2006). The P2X7 receptor: a key player in IL-1 processing and release. J. Immunol. *176*, 3877–3883.

Georgiev, H., Ravens, I., Papadogianni, G., Malissen, B., Förster, R., and Bernhardt, G. (2018). Blocking the ART2.2/P2X7-system is essential to avoid a detrimental bias in functional CD4 T cell studies. Eur. J. Immunol. *48*, 1078–1081.

Glowacki, G., Braren, R., Firner, K., Nissen, M., Kühl, M., Reche, P., Bazan, F., Cetkovic-Cvrlje, M., Leiter, E., Haag, F., and Koch-Nolte, F. (2002). The family of toxin-related ecto-ADP-ribosyltransferases in humans and the mouse. Protein Sci. *11*, 1657–1670.

Heiss, K., Jänner, N., Mähnss, B., Schumacher, V., Koch-Nolte, F., Haag, F., and Mittrücker, H.-W. (2008). High sensitivity of intestinal CD8+ T cells to nucleotides indicates P2X7 as a regulator for intestinal T cell responses. J. Immunol. *181*, 3861–3869.

Heng, T.S.P., Painter, M.W., and Immunological genome project consortium. (2008). The immunological genome project: networks of gene expression in immune cells. Nat. Immunol. *9*, 1091–1094.

Hubert, S., Rissiek, B., Klages, K., Huehn, J., Sparwasser, T., Haag, F., Koch-Nolte, F., Boyer, O., Seman, M., and Adriouch, S. (2010). Extracellular NAD+ shapes the Foxp3+ regulatory T cell compartment through the ART2-P2X7 pathway. J. Exp. Med. *207*, 2561–2568.

Kayagaki, N., Warming, S., Lamkanfi, M., Vande Walle, L., Louie, S., Dong, J., Newton, K., Qu, Y., Liu, J., Heldens, S., et al. (2011). Non-canonical inflammasome activation targets caspase-11. Nature *479*, 117–121.

Keane, T.M., Goodstadt, L., Danecek, P., White, M.A., Wong, K., Yalcin, B., Heger, A., Agam, A., Slater, G., Goodson, M., et al. (2011). Mouse genomic variation and its effect on phenotypes and gene regulation. Nature *477*, 289–294.

Kim, K.-D., Bae, S., Capece, T., Nedelkovska, H., de Rubio, R.G., Smrcka, A.V., Jun, C.-D., Jung, W., Park, B., Kim, T.-I., and Kim, M. (2017). Targeted calcium influx boosts cytotoxic T lymphocyte function in the tumour microenvironment. Nat. Commun. *8*, 15365.

Kim, K.-D., Srikanth, S., Tan, Y.-V., Yee, M.-K., Jew, M., Damoiseaux, R., Jung, M.E., Shimizu, S., An, D.S., Ribalet, B., et al. (2014). Calcium signaling via Orai1 is essential for induction of the nuclear orphan receptor pathway to drive Th17 differentiation. J. Immunol. *192*, 110–122.

Koch-Nolte, F., Reyelt, J., Schössow, B., Schwarz, N., Scheuplein, F., Rothenburg, S., Haag, F., Alzogaray, V., Cauerhff, A., and Goldbaum, F.A. (2007). Single domain antibodies from llama effectively and specifically block T cell ecto-ADP-ribosyltransferase ART2.2 in vivo. FASEB J. *21*, 3490–3498.

Kuida, K., Lippke, J.A., Ku, G., Harding, M.W., Livingston, D.J., Su, M.S., and Flavell, R.A. (1995). Altered cytokine export and apoptosis in mice deficient in interleukin-1 beta converting enzyme. Science *267*, 2000–2003.

Le Stunff, H., Auger, R., Kanellopoulos, J., and Raymond, M.-N. (2004). The Pro-451 to Leu polymorphism within the C-terminal tail of P2X7 receptor impairs cell death but not phospholipase D activation in murine thymocytes. J. Biol. Chem. *279*, 16918–16926.

Ledderose, C., Liu, K., Kondo, Y., Slubowski, C.J., Dertnig, T., Denicoló, S., Arbab, M., Hubner, J., Konrad, K., Fakhari, M., et al. (2018). Purinergic P2X4 receptors and mitochondrial ATP production regulate T cell migration. J. Clin. Invest. *128*, 3583–3594.

Lischke, T., Schumacher, V., Wesolowski, J., Hurwitz, R., Haag, F., Koch-Nolte, F., and Mittrücker, H.-W. (2013). CD8-β ADP-ribosylation affects CD8(+) T-cell function. Eur. J. Immunol. *43*, 1828–1838.

Lusis, A.J., Yu, J., and Wang, S.S. (2007). The problem of passenger genes in transgenic mice. Arterioscler. Thromb. Vasc. Biol. *27*, 2100–2103.

McCarl, C.-A., Khalil, S., Ma, J., Oh-hora, M., Yamashita, M., Roether, J., Kawasaki, T., Jairaman, A., Sasaki, Y., Prakriya, M., and Feske, S. (2010). Store-Operated Ca2+ entry through ORAI1 is critical for T cell-mediated autoimmunity and allograft rejection. J. Immunol. *185*, 5845–5858.

Mostafavi, S., Ortiz-Lopez, A., Bogue, M.A., Hattori, K., Pop, C., Koller, D., Mathis, D., Benoist, C., and Consortium, T.I.G. (2014). Variation and genetic control of gene expression in primary immunocytes across inbred mouse strains. J. Immunol. *193*, 4485–4496.

Nicke, A., Kuan, Y.-H., Masin, M., Rettinger, J., Marquez-Klaka, B., Bender, O., Górecki, D.C., Murrell-Lagnado, R.D., and Soto, F. (2009). A functional P2X7 splice variant with an alternative transmembrane domain 1 escapes gene inactivation in P2X7 knock-out mice. J. Biol. Chem. *284*, 25813–25822.

Nohara, L.L., Stanwood, S.R., Omilusik, K.D., and Jefferies, W.A. (2015). Tweeters, woofers and horns: the complex orchestration of calcium currents in T lymphocytes. Front. Immun. *6*, 234.

Proietti, M., Cornacchione, V., Rezzonico Jost, T., Romagnani, A., Faliti, C.E., Perruzza, L., Rigoni, R., Radaelli, E., Caprioli, F., Preziuso, S., et al. (2014). ATP-gated ionotropic P2X7 receptor controls follicular T helper cell numbers in Peyer's patches to promote host-microbiota mutualism. Immunity *41*, 789–801.

Rissiek, B., Danquah, W., Haag, F., and Koch-Nolte, F. (2014). Technical Advance: a new cell preparation strategy that greatly improves the yield of vital and functional Tregs and NKT cells. J. Leukoc. Biol. *95*, 543–549.

Rissiek, B., Haag, F., Boyer, O., Koch-Nolte, F., and Adriouch, S. (2015). P2X7 on mouse T cells: one channel, many functions. Front. Immun. *6*, 204.

Rissiek, B., Lukowiak, M., Haag, F., Magnus, T., and Koch-Nolte, F. (2018a). Monitoring the sensitivity of T cell populations towards NAD+ released during cell preparation. Methods Mol. Biol. *1813*, 317–326.

Rissiek, B., Lukowiak, M., Raczkowski, F., Magnus, T., Mittrücker, H.-W., and Koch-Nolte, F. (2018b). In vivo blockade of murine ARTC2.2 during cell preparation preserves the vitality and function of liver tissue-resident memory T cells. Front. Immun. *9*, 1580.

Rissiek, B., Menzel, S., Leutert, M., Cordes, M., Behr, S., Jank, L., Ludewig, P., Gelderblom, M., Rissiek, A., Adriouch, S., et al. (2017). Ecto-ADP-ribosyltransferase ARTC2.1 functionally modulates FcγR1 and FcγR2B on murine microglia. Sci. Rep. *7*, 16477.

Romagnani, A., Rottoli, E., Mazza, E.M.C., Rezzonico Jost, T., De Ponte Conti, B., Proietti, M., Perotti, M., Civanelli, E., Perruzza, L., Catapano, A.L., et al. (2020). P2X7 receptor activity limits accumulation of T cells within tumors. Cancer Res. *80*, 3906–3919.

Schenk, U., Westendorf, A.M., Radaelli, E., Casati, A., Ferro, M., Fumagalli, M., Verderio, C., Buer, J., Scanziani, E., and Grassi, F. (2008). Purinergic control of T cell activation by ATP released through pannexin-1 hemichannels. Sci. Signaling *1*, ra6.

Scheuplein, F., Schwarz, N., Adriouch, S., Krebs, C., Bannas, P., Rissiek, B., Seman, M., Haag, F., and Koch-Nolte, F. (2009). NAD+ and ATP released from injured cells induce P2X7-dependent shedding of CD62L and externalization of phosphatidylserine by murine T cells. J. Immunol. *182*, 2898–2908.

Schwarz, N., Drouot, L., Nicke, A., Fliegert, R., Boyer, O., Guse, A.H., Haag, F., Adriouch, S., and Koch-Nolte, F. (2012). Alternative splicing of the N-terminal cytosolic and transmembrane domains of P2X7 controls gating of the ion channel by ADP-ribosylation. PLoS One *7*, e41269.

Schwarz, N., Fliegert, R., Adriouch, S., Seman, M., Guse, A.H., Haag, F., and Koch-Nolte, F. (2009). Activation of the P2X7 ion channel by soluble and covalently bound ligands. Purinergic Signal. *5*, 139–149.

Seman, M., Adriouch, S., Scheuplein, F., Krebs, C., Freese, D., Glowacki, G., Deterre, P., Haag, F., and Koch-Nolte, F. (2003). NAD-induced T cell death: ADP-ribosylation of cell surface proteins by ART2 activates the cytolytic P2X7 purinoceptor. Immunity *19*, 571–582.

Silver, L.M. (1995). Mouse Genetics (Oxford University Press on Demand).

Sim, J.A., Chaumont, S., Jo, J., Ulmann, L., Young, M.T., Cho, K., Buell, G., North, R.A., and Rassendren, F. (2006). Altered hippocampal synaptic potentiation in P2X4 knock-out mice. J. Neurosci. *26*, 9006–9009.

Sorge, R.E., Trang, T., Dorfman, R., Smith, S.B., Beggs, S., Ritchie, J., Austin, J.-S., Zaykin, D.V., Vander Meulen, H., Costigan, M., et al. (2012). Genetically determined P2X7 receptor pore formation regulates variability in chronic pain sensitivity. Nat. Med. *18*, 595–599.

Stark, R., Wesselink, T.H., Behr, F.M., Kragten, N.A.M., Arens, R., Koch-Nolte, F., van Gisbergen, K.P.J.M., and van Lier, R.A.W. (2018). TRMmaintenance is regulated by tissue damage via P2RX7. Sci. Immunol. *3*, eaau1022.

Teege, S., Hann, A., Miksiewicz, M., MacMillan, C., Rissiek, B., Buck, F., Menzel, S., Nissen, M., Bannas, P., Haag, F., et al. (2015). Tuning IL-2 signaling by ADP-ribosylation of CD25. Sci. Rep. *5*, 8959.

Ventre, E., Rozières, A., Lenief, V., Albert, F., Rossio, P., Laoubi, L., Dombrowicz, D., Staels, B., Ulmann, L., Julia, V., et al. (2017). Topical ivermectin improves allergic skin inflammation. Allergy *72*, 1212–1221.

Vig, M., DeHaven, W.I., Bird, G.S., Billingsley, J.M., Wang, H., Rao, P.E., Hutchings, A.B., Jouvin, M.-H., Putney, J.W., and Kinet, J.-P. (2008). Defective mast cell effector functions in mice lacking the CRACM1 pore subunit of store-operated calcium release-activated calcium channels. Nat. Immunol. *9*, 89–96.

iScience, Volume *23*

Supplemental Information

A *P2rx7* Passenger Mutation Affects the Vitality and Function of T cells in Congenic Mice

Marco Er-Lukowiak, Yinghui Duan, Francois Rassendren, Lauriane Ulmann, Annette Nicke, Friederike Ufer, Manuel A. Friese, Friedrich Koch-Nolte, Tim Magnus, and Björn Rissiek

Transparent Methods

Mice

8 to 18 weeks old male and female mice on the C57BL/6 and Balb/c background were used in this study. P2rx4^{tm1Rass} on the B6 background were obtained from the lab of Francois Rassendren. Balb/c-P2X4^{-}ko mice were generated by backcrossing B6-P2X4ko mice with Balb/c-WT mice for 13 generations. In some experiments cells from B6-P2X7ko mice (P2rx7^{tm1Gab}) were used as negative control for P2X7 cell surface staining. Hvcn1$^{Gt(RRRN293)Byg}$ on the B6 background were obtained from the lab of David Clapham. All mouse experiments were approved by the responsible regulatory committee (Hamburger Behörde für Gesundheit und Verbraucherschutz, Veterinärwesen/Lebensmittelsicherheit, ORG722, ORG983, G12/130). All experiments were performed according to the relevant guidelines and regulations.

Antibodies and flow cytometry

For FACS analysis, the following antibodies were used: anti-CD3-Bv421-(clone 17A2, Biolegend), anti-CD4-Bv421 (clone RM 4-5, eBioscience), anti-CD8-FITC (clone 53-6.7, Biolegend), anti-CD25 PE (clone PC61, Biolegend), anti-CD27-APC (clone LG.3A10, Biolegend) and anti-P2X7-AF647 (clone Hano44, UKE) (Adriouch et al. 2005). Flow cytometric analyses were performed on a BD Fortessa (Beckton Dickinson) or a BD FACS CantoII (Beckton Dickinson).

Preparation of immune cells

The isolation of immune cells was performed strictly at 4°C on ice. Spleen and peripheral lymph nodes were mashed through a cell strainer (50 mL falcon strainer, 70 µm, GBO) using a syringe piston. Single cell suspension was kept in FACS buffer containing 1 mM EDTA (Sigma) and 0.1 % bovine serum albumin (Sigma). Erythrocytes were lysed using an ACK lysis buffer (155 mM NH_4Cl, 10 mM $KHCO_3$, 0.1 mM EDTA, pH 7.2). For some T cell experiments, mice were injected (i.v.) with 50 µg of the ARTC2.2-blocking nanobody s+16a 30 min prior to sacrificing the mice in order to prevent ADP-ribosylation of P2X7 on T cells during cell preparation.

Quantitative real-time PCR

RNA was extracted from FACS sorted immune cells using the RNeasy Plus Mini Kit (Qiagen) followed by cDNA synthesis using the Maxima First Strand cDNA Synthesis Kit (Thermo Fisher Scientific) as recommended by the respective supplier. RT-qPCR was performed on a Lightcycler 96 (Roche). A *P2rx7*-specific Taqman probe (Mm00440582_m1; Thermo Scientific) was used to determine *P2rx7* mRNA expression levels.

P2rx7 SNP sequencing

Sequencing of a region flanking SNP rs48804829 in the *P2rx7* gene was performed using the primers P2x7_P451L_forw (gggaaaagtctgcaagttgtc) and P2x7_P451L_rev (gaagagcttggaggtggtg). The PCR product was purified with the PCR clean-up gel extraction kit (Macherey-Nagel) and send to Eurofins, Germany, for sequencing.

Monitoring P2X7 induced cell death on T cells

T cells were isolated by flow cytometric cell sorting. 5 x 10^4 cell were resuspended in 400 µl complete RPMI medium containing propidium iodide PI (2.5 µg/ml, ImmunoChemistry Technologies). Half of the sample was left at 4°C and the other half was incubated for 2 h at 37°C. Cell vitality was analyzed directly after incubation by flow cytometry.

Monitoring P2X7 shedding of CD27 on T cells

Purified splenocytes from WT and P2X4ko mice were stained with lineage markers and anti-CD27 for 30 min, then washed and WT or P2X4ko cells were labeled with eFluor^{670}. The labeled and unlabeled samples were mixed in a 1:1 ratio and aliquots were subjected to ATP dose response analyses (16-500 µM ATP). For this, cells were incubated in the presence of ATP at 37°C for 15 minutes, samples without ATP were incubated at 4°C and 37°C as controls. Loss of CD27 from the cell surface was analyzed by flow cytometry.

For the real-time CD27 shedding measurements, WT or P2X4ko cells were labeled with eFluor^{670}. The labeled and unlabeled samples were mixed in a 1:1 ratio and aliquots and cell surface CD27expression was monitored on a flow cytometer while continuously increasing the sample temperature to 37°C using an infrared lamp (IR) lamp. A temperature of 37°C was reached after 7-8 min and kept constant while measuring continued for another 7-8 minutes

Monitoring P2X7-induced calcium uptake

HEK cells stably transfected with expression plasmids for P2X7k 451L, P2X7k 451P, P2X7a 451L or P2X7a 451P were loaded with 2 µM Fluo-4 (Invitrogen) for 20 min at 4°C and 10 min at 37°C, washed once with FACS buffer and resuspended in PBS supplemented with 0.9 mM $CaCl_2$ and 0.49 mM $MgCl_2$ (Invitrogen) and analyzed by flow cytometry. An IR lamp was used to maintain a constant sample temperature of 37°C. The baseline Fluo4 signal was measured for 2 minutes, then ATP was added to the sample at the indicated concentration and measuring continued for 3-4 minutes.

In vitro migration assay

Th were isolated from WT and P2X4ko mice by FACS and one WT or P2X4ko Th were stained witheFluor^{670}. Labeled and unlabeled cells were mixed in a 1:1 ratio, washed and resuspended in RPMI complete medium. 2 x 10^5 cells in 100 µl were transferred into the upper chamber of a trans-well plate (5µm pores, Corning). The lower chamber was prepared with either 150 µl RPMI complete medium or 150 µl RPMI complete medium containing SDF1α (100 ng/ml, Biolegend). The trans-well plate was placed in a 37°C incubator and cells were allowed to migrate for 2 h. Afterwards, vital cells (propidium iodide negative) in the upper and lower chamber were counted by flow cytometry.

Cytokine secretion assay

For *in vitro* cytokine secretion assays CTL were isolated by FACS from spleen single cell suspensions. 5 x 10^4 cells were directly sorted in 200 µl RPMI complete medium and stimulated for 24 h in the presence of phorbol 12-myristate 13-acetate (PMA, 20 ng/ml, Invivogen) and ionomycin (1 µg/ml, Invivogen). Supernatants were analyzed for 13 cytokines (IFN-γ, TNF-α, IL-2, IL-4, IL-21, IL-22, IL-17A, IL-17F, IL-10, IL-9, IL-5 and IL-13) using the LEGENDplex mouse Th cytokine 13-plex kit (Biolegend).

In silico research and statistics

mRNA sequencing data from CD4 T cells of inbred mouse strains was obtained from the immgen database (GSE60337) (Mostafavi et al. 2014). Details of *P2rx7* neighboring genes were obtained from BioMart on ensembl.org (Yates et al. 2020). For statistical analyses, GraphPad Prism 8 was used and two groups were compared using the student's t test.

References Transparent Methods

Adriouch, S. et al., 2005. Probing the expression and function of the P2X7 purinoceptor with antibodies raised by genetic immunization. *Cellular Immunology*, 236(1-2), pp.72–77.

Mostafavi, S. et al., 2014. Variation and Genetic Control of Gene Expression in Primary Immunocytes across Inbred Mouse Strains. *Journal of Immunology*, 193(9), pp.4485–4496.

Yates, A.D. et al., 2020. Ensembl 2020. *Nucleic acids research*, 48(D1), pp.D682–D688.

Supplementary Figures

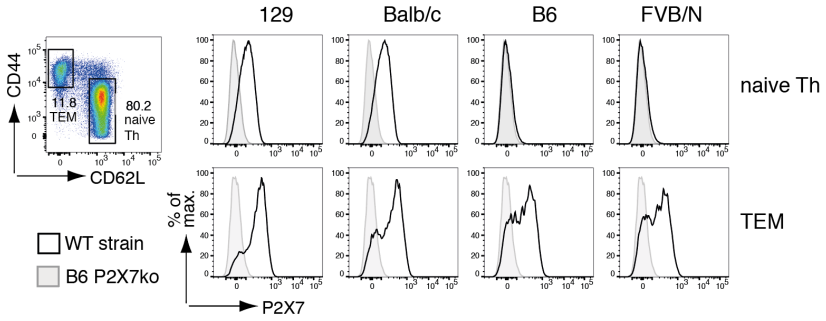

Figure S1. P2X7 expression levels in naïve and effector/memory T cells (TEM) from different mouse strains. Related to Figure 1. Flow cytometric analyses of cell surface P2X7 expression on $CD4^+$ naïve ($CD62L+CD44^{low}$) and effector/memory ($CD62L^-CD44^{high}$) $CD4^+$ T cells (TEM) of 129, Balb/c, B6 and FVB/N mice.

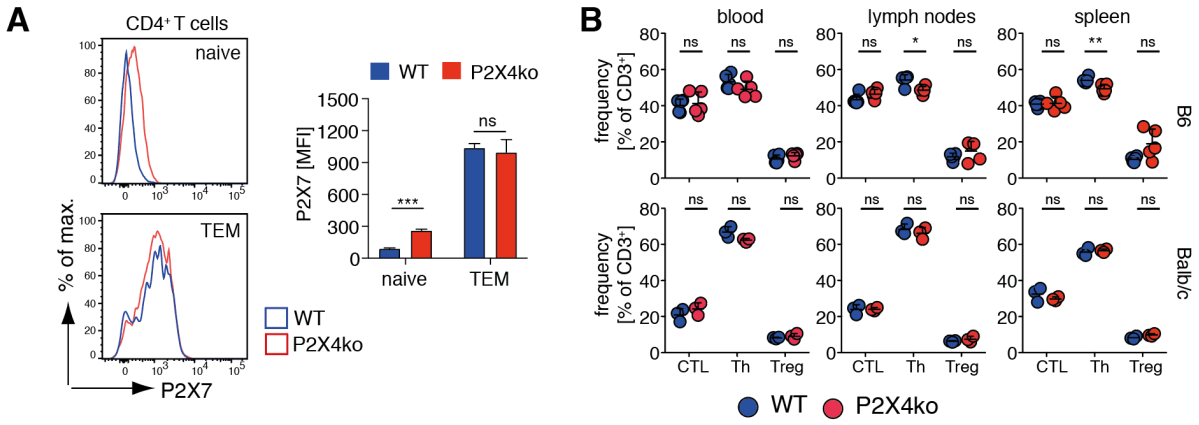

Figure S2. Naïve and effector memory T cells P2X7 expression analyses and T cell frequencies in P2X4ko and WT mice. Related to Figure 2. **(A)** Flow cytometric analyses of cell surface P2X7 expression on $CD4^+$ naïve ($CD62L+CD44^{low}$) and effector/memory ($CD62L^-CD44^{high}$) T cells of B6 WT (blue) and P2X4ko (red) mice. **(B)** Frequencies of CTL, Th and Treg (n = 3-5) in relation to all $CD3^+$ T cells was determined in blood, peripheral lymph nodes and spleen of B6 and Balb/c P2X4ko (red) and WT mice (blue). Data are represented as mean +/– SD. Statistical comparison of two groups was performed by using the student's t test ($p < 0.05$ = * / $p < 0.01$ = ** / $p < 0.001$ = ***, ns = no significant).

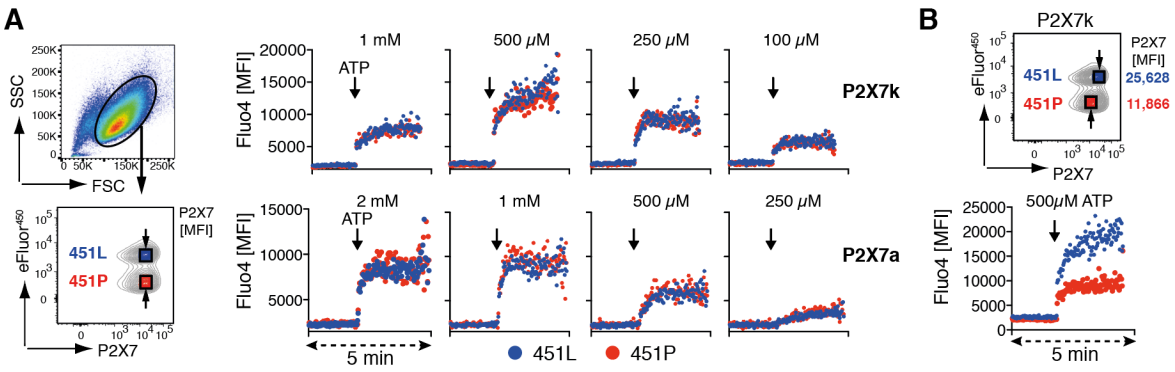

Figure S3. The intensity of the calcium influx depends on the expression level of P2X7. Related to Figure 3. **(A)** HEK cells stably transfected with P2X7 451L or 451P (P2X7k or P2X7a splice variant) were distinguished by eFluor^{450} labeling and P2X7 expression level were determined by co-staining with an anti-P2X7 antibody (clone RH23A44). Comparative P2X7 451P/L HEK cell analyses were adjusted for P2X7 expression levels by creating a gating region with a comparable P2X7 mean fluorescence intensity (MFI). For the analyses, mixed HEK cells were loaded with Fluo4 and measured in a real-time flow cytometry assay with 2 min baseline recording followed by 3 min ATP stimulation (100 µM – 2 mM). Calcium influx was measured by increase in Fluo4 MFI. **(B)** Analysis of the 500 µM ATP P2X7k sample was repeated with a skewed adjustment of P2X7 expression.

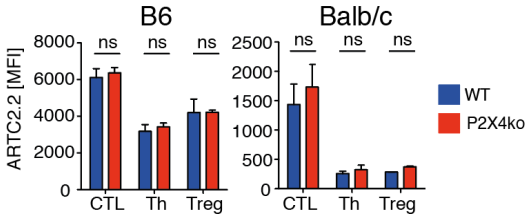

Figure S4. ARTC2.2 expression is comparable on P2X4ko and WT T cells. Related to Figure 3. Flow cytometric analyses of cell surface ARTC2.2 expression on CTL, Th and Treg of WT and P2X4ko mice on the B6 and Balb/c background. The mean fluorescence intensity (MFI) of ARTC2.2 on the different T cell populations from WT and P2X4ko mice (n = 3) was compared. Data are represented as mean +/– SD. Statistical comparison of two groups was performed by using the student's t test ($p < 0.05$ = * / $p < 0.01$ = ** / $p < 0.001$ = ***, ns = no significant).

Table S1: 129-based knockout mice for *P2rx7* neighboring genes. Related to Figure 6.

gene name	gene start (bp)	gene end (bp)	distance to P2rx7 (bp)	gene description	129-based KO mice
Rasal1	120648812	120679597	-1964314	RAS protein activator like 1 (GAP1 like) [Source:MGI Symbol;Acc:MGI:1330842]	---
Dtx1	120680202	120711927	-1931984	deltex 1, E3 ubiquitin ligase [Source:MGI Symbol;Acc:MGI:1352744]	Dtx1tm1.1Mzl Dtx1tm1Crey Dtx1tm1Mjb
Oas2	120730333	120749853	-1894058	2'-5' oligoadenylate synthetase 2 [Source:MGI Symbol;Acc:MGI:2180852]	Oas2Gt(OST112989)Lex
Oas3	120753098	120777661	-1866250	2'-5' oligoadenylate synthetase 3 [Source:MGI Symbol;Acc:MGI:2180850]	---
Oas1e	120786226	120795530	-1848381	2'-5' oligoadenylate synthetase 1E [Source:MGI Symbol;Acc:MGI:2180856]	---
Oas1c	120800194	120812514	-1831397	2'-5' oligoadenylate synthetase 1C [Source:MGI Symbol;Acc:MGI:2149633]	---
Oas1b	120812635	120824163	-1819748	2'-5' oligoadenylate synthetase 1B [Source:MGI Symbol;Acc:MGI:97430]	Oas1btm1.1Brin
Oas1f	120847367	120857986	-1785925	2'-5' oligoadenylate synthetase 1F [Source:MGI Symbol;Acc:MGI:2180855]	Oas1fGt(OST425760)Lex
Oas1h	120861421	120873506	-1770405	2'-5' oligoadenylate synthetase 1H [Source:MGI Symbol;Acc:MGI:2180853]	---
Oas1g	120876142	120887613	-1756298	2'-5' oligoadenylate synthetase 1G [Source:MGI Symbol;Acc:MGI:97429]	---
Oas1a	120896256	120907521	-1736390	2'-5' oligoadenylate synthetase 1A [Source:MGI Symbol;Acc:MGI:2180860]	---
Oas1d	120914536	120921652	-1722259	2'-5' oligoadenylate synthetase 1D [Source:MGI Symbol;Acc:MGI:2140770]	Oas1dtm1Zuk
Rph3a	120940499	121010092	-1633819	rabphilin 3A [Source:MGI Symbol;Acc:MGI:102788]	Rph3atm1Sud
Ptpn11	121130533	121191397	-1452514	protein tyrosine phosphatase, non-receptor type 11 [Source:MGI Symbol;Acc:MGI:99511]	Ptpn11tm1.1Rbns Ptpn11tm1.1Wbm Ptpn11tm1Bgn Ptpn11tm1Rbn Ptpn11tm1Yan
Rpl6	121204481	121209241	-1434670	ribosomal protein L6 [Source:MGI Symbol;Acc:MGI:108057]	Rpl6Gt(OST1622)Lex Rpl6Gt(PST17838)Mfgc
Hectd4	121220219	121368577	-1275334	HECT domain E3 ubiquitin protein ligase 4 [Source:MGI Symbol;Acc:MGI:3647820]	Hectd4Gt(255G8)Cmhd Hectd4Gt(BC0299)Wtsi Hectd4Gt(BGA536)Byg
Trafd1	121371725	121385632	-1258279	TRAF type zinc finger domain containing 1 [Source:MGI Symbol;Acc:MGI:1923551]	Trafd1tm1Ayos
Naa25	121397936	121444378	-1199533	N(alpha)-acetyltransferase 25, NatB auxiliary subunit [Source:MGI Symbol;Acc:MGI:2442563]	Naa25Gt(RRK280)Byg Naa25Gt(AL0004)Wtsi
Erp29	121428590	121452506	-1191405	endoplasmic reticulum protein 29 [Source:MGI Symbol;Acc:MGI:1914647]	Erp29tm1Dfer Erp29Gt(KST171)Byg Erp29Gt(G014A01)Wrst
Tmem116	121451893	121524183	-1119728	transmembrane protein 116 [Source:MGI Symbol;Acc:MGI:1924712]	Tmem116Gt(OST44984)Lex Tmem116Gt(PST12765)Mfgc
Adam1b	121500098	121503435	-1140476	a disintegrin and metallopeptidase domain 1b [Source:MGI Symbol;Acc:MGI:2429506]	---
Adam1a	121518576	121545482	-1098429	a disintegrin and metallopeptidase domain 1a [Source:MGI Symbol;Acc:MGI:2429504]	Adam1btm1Tba
Mapkapk5	121525038	121545905	-1098006	MAP kinase-activated protein kinase 5 [Source:MGI Symbol;Acc:MGI:1333110]	Mapkapk5tm1Mgl Mapkapk5tm1Pqs
Aldh2	121566027	121593824	-1050087	aldehyde dehydrogenase 2, mitochondrial [Source:MGI Symbol;Acc:MGI:99600]	Aldh2Gt(OST7285)Lex Aldh2Gt(D053A10)Wrst
Acad12	121596775	121618938	-1024973	acyl-Coenzyme A dehydrogenase family, member 12 [Source:MGI Symbol;Acc:MGI:2443320]	Acad12Gt(OST300106)Lex
Acad10	121621026	121660514	-983397	acyl-Coenzyme A dehydrogenase family, member 10 [Source:MGI Symbol;Acc:MGI:1919235]	Acad10Gt(OST448289)Lex
Brap	121660563	121687256	-956655	BRCA1 associated protein [Source:MGI Symbol;Acc:MGI:1919649]	---
Atxn2	121711337	121816493	-827418	ataxin 2 [Source:MGI Symbol;Acc:MGI:1277223]	Atxn2tm1.1Geno Atxn2tm1Plt Atxn2tm2.1Geno Atxn2tm1.1Aub Atxn2tm2.1Aub Atxn2tm3.1Aub Atxn2Gt(A014A02)Wrst
Sh2b3	121815488	121837646	-806265	SH2B adaptor protein 3 [Source:MGI Symbol;Acc:MGI:893598]	Sh2b3tm1Paw Sh2b3tm1Rmp
Pheta1	121848984	121854632	-789279	PH domain containing endocytic trafficking adaptor 1 [Source:MGI Symbol;Acc:MGI:2442708]	---
Cux2	121856366	122050102	-593809	cut-like homeobox 2 [Source:MGI Symbol;Acc:MGI:107321]	Cux2tm1.1Nieto
Myl2	122100951	122113472	-530439	myosin, light polypeptide 2, regulatory, cardiac, slow [Source:MGI Symbol;Acc:MGI:97272]	Myl2tm1(cre)Krc Myl2tm1(Hand1)Tana Myl2tm1.1Chen Myl2tm2.1Chen
Ccdc63	122108040	122140823	-503088	coiled-coil domain containing 63 [Source:MGI Symbol;Acc:MGI:3607777]	---
Ppp1cc	122158278	122175273	-468638	protein phosphatase 1 catalytic subunit gamma [Source:MGI Symbol;Acc:MGI:104872]	Ppp1cctm1Lex Ppp1cctm1Var
Hvcn1	122206804	122242297	-401614	hydrogen voltage-gated channel 1 [Source:MGI Symbol;Acc:MGI:1921346]	Hvcn1Gt(RRN293)Byg
Tctn1	122237848	122264460	-379451	tectonic family member 1 [Source:MGI Symbol;Acc:MGI:3603820]	---
Pptc7	122284365	122324281	-319630	PTC7 protein phosphatase homolog [Source:MGI Symbol;Acc:MGI:2444593]	---
Rad9b	122323223	122354233	-289678	RAD9 checkpoint clamp component B [Source:MGI Symbol;Acc:MGI:2385231]	Rad9btm1Lieb
Vps29	122354369	122364984	-278927	VPS29 retromer complex component [Source:MGI Symbol;Acc:MGI:1928344]	Vps29Gt(OST309649)Lex

Fam216a	122364580	122372364	-271547	family with sequence similarity 216, member A [Source:MGI Symbol;Acc:MGI:1916198]	---
Gpn3	122371876	122382902	-261009	GPN-loop GTPase 3 [Source:MGI Symbol;Acc:MGI:1289326]	---
Arpc3	122391878	122414184	-229727	actin related protein 2/3 complex, subunit 3 [Source:MGI Symbol;Acc:MGI:1928375]	Arpc3tm1Jtak
Anapc7	122421693	122444912	-198999	anaphase promoting complex subunit 7 [Source:MGI Symbol;Acc:MGI:1929711]	---
Atp2a2	122453513	122502225	-141686	ATPase, Ca++ transporting, cardiac muscle, slow twitch 2 [Source:MGI Symbol;Acc:MGI:88110]	Atp2a2tm1.1Iemr Atp2a2tm1Fwuy Atp2a2tm1Ges
Ift81	122550204	122614518	-29393	intraflagellar transport 81 [Source:MGI Symbol;Acc:MGI:1098597]	---
P2rx7	**122643911**	**122691432**	**0**	**purinergic receptor P2X, ligand-gated ion channel, 7 [Source:MGI Symbol;Acc:MGI:1339957]**	P2rx7tm1Lex P2rx7tm1Gab P2rx7tm1.2Jde P2rx7Gt(OST90373)Lex
P2rx4	122707544	122729738	16112	purinergic receptor P2X, ligand-gated ion channel 4 [Source:MGI Symbol;Acc:MGI:1338859]	P2rx4tm1Rass P2rx4tm1Dgen
Camkk2	122731170	122779409	39738	calcium/calmodulin-dependent protein kinase kinase 2, beta [Source:MGI Symbol;Acc:MGI:2444812]	Camkk2tm1Kpg Camkk2tm1Shyy Camkk2tm1Tch Camkk2tm2.1Kpg Camkk2tm2Kpg
Anapc5	122787459	122821339	96027	anaphase-promoting complex subunit 5 [Source:MGI Symbol;Acc:MGI:1929722]	---
Rnf34	122850048	122871291	158616	ring finger protein 34 [Source:MGI Symbol;Acc:MGI:2153340]	---
Kdm2b	122870665	122989823	179233	lysine (K)-specific demethylase 2B [Source:MGI Symbol;Acc:MGI:1354737]	Kdm2btm1.1Atz Kdm2btm1.1Bes Kdm2btm1Nobu
Orai1	123015074	123030456	323642	ORAI calcium release-activated calcium modulator 1 [Source:MGI Symbol;Acc:MGI:1925542]	Orai1tm1.1Ygwa
Morn3	123035769	123047016	344337	MORN repeat containing 3 [Source:MGI Symbol;Acc:MGI:1922140]	---
Tmem120b	123068415	123117749	376983	transmembrane protein 120B [Source:MGI Symbol;Acc:MGI:3603158]	---
Rhof	123103044	123132692	411612	ras homolog family member F (in filopodia) [Source:MGI Symbol;Acc:MGI:1345629]	---
Setd1b	123142193	123168629	450761	SET domain containing 1B [Source:MGI Symbol;Acc:MGI:2652820]	Setd1btm1.1Afst Setd1btm1Afst
Psmd9	123169413	123250131	477981	proteasome (prosome, macropain) 26S subunit, non-ATPase, 9 [Source:MGI Symbol;Acc:MGI:1914401]	---
Hpd	123171807	123182727	480375	4-hydroxyphenylpyruvic acid dioxygenase [Source:MGI Symbol;Acc:MGI:96213]	---
Wdr66	123252102	123327484	560670	WD repeat domain 66 [Source:MGI Symbol;Acc:MGI:1918495]	---
Bcl7a	123343834	123374992	652402	B cell CLL/lymphoma 7A [Source:MGI Symbol;Acc:MGI:1924295]	---
Mlxip	123394798	123457932	703366	MLX interacting protein [Source:MGI Symbol;Acc:MGI:2141183]	Mlxiptm1.1Lchan Mlxiptm1.2Lchan
Rpl31-ps6	123466509	123466886	775077	ribosomal protein L31, pseudogene 6 [Source:MGI Symbol;Acc:MGI:3783190]	---
Il31	123480157	123489489	788725	interleukin 31 [Source:MGI Symbol;Acc:MGI:1923649]	---
Lrrc43	123489305	123508205	797873	leucine rich repeat containing 43 [Source:MGI Symbol;Acc:MGI:2685907]	---
Diablo	123509765	123524176	818333	diablo, IAP-binding mitochondrial protein [Source:MGI Symbol;Acc:MGI:1913843]	Diablotm1Mak
B3gnt4	123510460	123511882	819028	UDP-GlcNAc:betaGal beta-1,3-N-acetylglucosaminyltransferase 4 [Source:MGI Symbol;Acc:MGI:2680208]	---
Vps33a	123528659	123573038	837227	VPS33A CORVET/HOPS core subunit [Source:MGI Symbol;Acc:MGI:1924823]	---
Clip1	123577795	123684618	886363	CAP-GLY domain containing linker protein 1 [Source:MGI Symbol;Acc:MGI:1928401]	Clip1tm1.1Gal Clip1tm1Gal
Zcchc8	123698294	123721100	1006862	zinc finger, CCHC domain containing 8 [Source:MGI Symbol;Acc:MGI:1917900]	---
Rsrc2	123728426	123749414	1036994	arginine/serine-rich coiled-coil 2 [Source:MGI Symbol;Acc:MGI:1913489]	---
Kntc1	123749716	123821593	1058284	kinetochore associated 1 [Source:MGI Symbol;Acc:MGI:2673709]	Kntc1Gt(OST40060)Lex
Hcar2	123863570	123865499	1172138	hydroxycarboxylic acid receptor 2 [Source:MGI Symbol;Acc:MGI:1933383]	Hcar2tm1Lex Hcar2tm1Soff
Hcar1	123876736	123880020	1185304	hydrocarboxylic acid receptor 1 [Source:MGI Symbol;Acc:MGI:2441671]	---
Denr	123907175	123928835	1215743	density-regulated protein [Source:MGI Symbol;Acc:MGI:1915434]	DenrGt(CSI770)Byg DenrGt(OST114)Lex
Ccdc62	123930679	123969895	1239247	coiled-coil domain containing 62 [Source:MGI Symbol;Acc:MGI:2684996]	---
Hip1r	123973628	124005558	1282196	huntingtin interacting protein 1 related [Source:MGI Symbol;Acc:MGI:1352504]	Hip1rtm1Tsr
Vps37b	124004641	124032270	1313209	vacuolar protein sorting 37B [Source:MGI Symbol;Acc:MGI:1916724]	---
Abcb9	124061530	124095798	1370098	ATP-binding cassette, sub-family B (MDR/TAP), member 9 [Source:MGI Symbol;Acc:MGI:1861729]	Abcb9Gt(231G11)Cmhd
Ogfod2	124112297	124115483	1420865	2-oxoglutarate and iron-dependent oxygenase domain containing 2 [Source:MGI Symbol;Acc:MGI:1913877]	---
Arl6ip4	124116089	124118196	1424657	ADP-ribosylation factor-like 6 interacting protein 4 [Source:MGI Symbol;Acc:MGI:1929500]	Arl6ip4Gt(OST31151)Lex
Pitpnm2	124118690	124249760	1427258	phosphatidylinositol transfer protein, membrane-associated 2 [Source:MGI Symbol;Acc:MGI:1336192]	Pitpnm2tm1Tili
Pitpnm2os2	124194907	124200346	1503475	phosphatidylinositol transfer protein, membrane-associated 2, opposite strand 2 [Source:MGI Symbol;Acc:MGI:3840147]	---
Pitpnm2os1	124229725	124237137	1538293	phosphatidylinositol transfer protein, membrane-associated 2, opposite strand 1 [Source:MGI Symbol;Acc:MGI:1923177]	---

Mphosph9	124250959	124327972	1559527	M-phase phosphoprotein 9 [Source:MGI Symbol;Acc:MGI:2443138]	Mphosph9Gt(OST104880)Lex
Cdk2ap1	124345417	124363082	1653985	CDK2 (cyclin-dependent kinase 2)-associated protein 1 [Source:MGI Symbol;Acc:MGI:1202069]	Cdk2ap1tm1Dtw Cdk2ap1Gt(D133C05)Wrst Cdk2ap1Gt(OST35764)Lex
Sbno1	124368702	124426001	1677270	strawberry notch 1 [Source:MGI Symbol;Acc:MGI:2384298]	Sbno1Gt(OST114991)Lex
Kmt5a	124439930	124462308	1748498	lysine methyltransferase 5A [Source:MGI Symbol;Acc:MGI:1915206]	Kmt5atm1.1Dare Kmt5aGt(RRB075)Byg Kmt5aGt(305D01)Cmhd Kmt5aGt(D060E05)Wrst Kmt5aGt(OST1973)Lex
Rilpl2	124463265	124478366	1771833	Rab interacting lysosomal protein-like 2 [Source:MGI Symbol;Acc:MGI:1933112]	Rilpl2Gt(OST96650)Lex Rilpl2Gt(450F7)Cmhd
Snrnp35	124483134	124491124	1791702	small nuclear ribonucleoprotein 35 (U11/U12) [Source:MGI Symbol;Acc:MGI:1923417]	Snrnp35Gt(D178F04)Wrst Snrnp35Gt(OST56118)Lex
Rilpl1	124493080	124531391	1801648	Rab interacting lysosomal protein-like 1 [Source:MGI Symbol;Acc:MGI:1922945]	Rilpl1Gt(209A4)Cmhd Rilpl1Gt(OST684)Lex
Tmed2	124540695	124550506	1849263	transmembrane p24 trafficking protein 2 [Source:MGI Symbol;Acc:MGI:1929269]	Tmed2Gt(OST78169)Lex
Ddx55	124552864	124569660	1861432	DEAD (Asp-Glu-Ala-Asp) box polypeptide 55 [Source:MGI Symbol;Acc:MGI:1915098]	Ddx55Gt(CSH561)Byg Ddx55Gt(OST406009)Lex
Eif2b1	124570213	124579131	1878781	eukaryotic translation initiation factor 2B, subunit 1 (alpha) [Source:MGI Symbol;Acc:MGI:2384802]	Eif2b1Gt(OST132125)Lex
Gtf2h3	124579140	124597680	1887708	general transcription factor IIH, polypeptide 3 [Source:MGI Symbol;Acc:MGI:1277143]	Gtf2h3Gt(D144D12)Wrst Gtf2h3Gt(RRG412)Byg
Tctn2	124598749	124627738	1907317	tectonic family member 2 [Source:MGI Symbol;Acc:MGI:1915228]	Tctn2tm1.1Reit Tctn2Gt(OST378011)Lex
Atp6v0a2	124628576	124724455	1937144	ATPase, H+ transporting, lysosomal V0 subunit A2 [Source:MGI Symbol;Acc:MGI:104855]	---